Electronic Supplementary Information

A Molecular Electron Density Theory Study of the [3+2] Cycloaddition Reaction of Nitrones with Strained Allenes

Luis R. Domingo,*[a] Mar Ríos-Gutiérrez[a] and Patricia Pérez[b]

[a] Department of Organic Chemistry, University of Valencia, Dr. Moliner 50, E-46100 Burjassot, Valencia, Spain.
[b] Universidad Andres Bello, Facultad de Ciencias Exactas, Departamento de Ciencias Químicas, Millennium Nucleus Chemical Processes and Catalysis (CPC), Av. República 498, 8370146, Santiago, Chile.
e-mail: domingo@utopia.uv.es
web: www.luisrdomingo.com

Index

S2 Study of the reaction paths associated with the [3+2] cycloaddition (32CA) reaction between nitrone **15** and the simplest linear allene **18**.
S5 BET study of the regioisomeric *r1* reactive channel associated with the 32CA reaction between nitrone **15** and the simplest allene **18**.
S13 BET study of the *endo/r1* reactive channel associated with the 32CA reaction between nitrone **15** and strained allene CHDE **10**.
S22 ELF topological analysis along the *exo/r1* reactive channel associated with the 32CA reaction between nitrone **15** and strained allene CHDE **10**.
S25 Theoretical background.
S25 Topological analysis of the electron localisation function (ELF)
S26 Bonding Evolution Theory (BET).
S28 References.
S30 **Table S5** with B3LYP/6-311G(d,p) thermodynamic data, computed at 80 ºC and 1 atm in acetonitrile, of the stationary points involved in the 32CA reaction of nitrone **15** with CHDE **10**.
S31 Analysis of the dependence of the thermodynamic data associated with the 32CA reaction between nitrone **15** and CHDE **10** with the DFT functional.
S35 **Table S9** with the B3LYP/6-311G(d,p) total and relative energies, in gas phase and in acetonitrile, of the stationary points involved in the 32CA reaction of nitrone **15** with CHDE **10**.
S35 **Table S10** with the B3LYP/6-311G(d,p) total and relative energies, in gas phase and in acetonitrile, of the stationary points involved in the 32CA reaction of nitrone **15** with the simplest allene **18**.
S36 **Figure S10** showing the relative energy variations along the IRC associated with the *endo/r1* and *exo/r1* reactive channels of the 32CA reaction between nitrone **15** and strained allene CHDE **10**, in gas phase and in acetonitrile.
S37 B3LYP/6-311G(d,p) computed total energies, unique imaginary frequencies and Cartesian coordinates in acetonitrile of the structures involved in the 32CA reaction between nitrone **15** and strained allene CHDE **10**.

*1. Study of the reaction paths associated with the [3+2] cycloaddition (32CA) reaction between nitrone **15** and the simplest linear allene **18**.*

The 32CA reaction of nitrone **15** with the simplest linear allene **18** was studied as a reaction model of nitrones with allenes. Due to the symmetry of the simplest allene **18**, the 32CA reaction between nitrone **15** and allene **18** can take place along two regioisomeric channels. They are related with the formation of the C1−C5 single bond, *channel r1*, and the formation of the O3−C5 single bond, *channel r2*. Analysis of the reaction path associated with the two regioisomeric channels indicates that this 32CA reaction takes place through a one-step mechanism. Consequently, the reagents, two TSs, **TS1** and **TS2**, and two isoxazolidine, **19** and **20**, associated with the two regioisomeric channels, were located and characterised (see Scheme S1). Thermodynamic data of the stationary points involved in the 32CA reaction of nitrone **15** with the simplest allene **18** are given in Table S1, while the total and relative energies are given in Table S10.

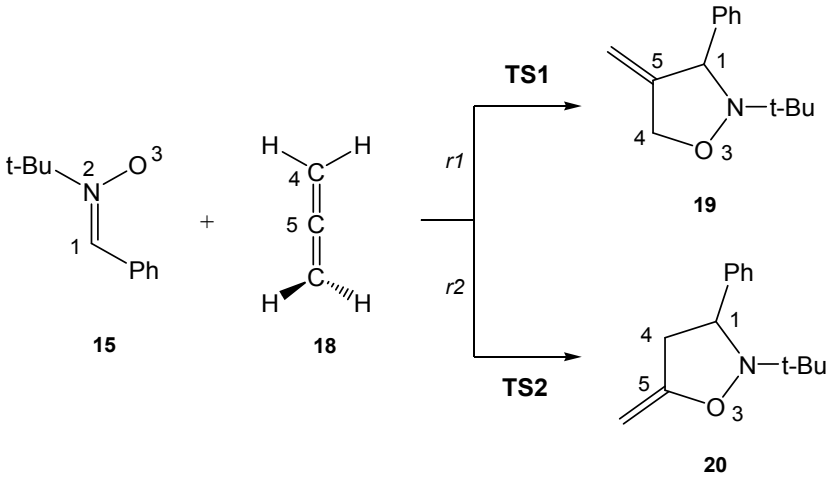

Scheme S1. 32CA reaction of nitrone **15** with the simplest allene **18**.

The activation Gibbs free energies associated with the two competitive regioisomeric channels are 44.5 (**TS1**) and 42.6 (**TS2**) kcal·mol^{-1}; while formation of **19** kcal·mol^{-1}is endergonic by 3.3 kcal·mol^{-1}, formation of **20** is exergonic by −4.3 kcal·mol^{-1}. Some appealing conclusions can be drawn from these relative energies: i) the non-polar 32CA reaction of nitrone **15** with allene **18** presents a very high activation Gibbs free energy, 42.6 (**TS2**) kcal·mol^{-1}, as a consequence of the poor electrophilic character of the simplest allene **18**; ii) this 32CA presents a low regioselectivity as **TS2** is only 1.9 kcal·mol^{-1} lower in energy than **TS1**; and iii) formation of isoxazolidine **20**

is thermodynamically favourable by 4.3 kcal·mol^{-1}, while formation of isoxazolidine **19** is unfavourable.

Table S1. B3LYP/6-311G(d,p) enthalpies (H, in au), entropies (S, in cal·mol^{-1}·K^{-1}) and Gibbs free energies (G, in au); and relative[a] enthalpies (ΔH, in kcal·mol^{-1}), entropies (ΔS, in cal·mol^{-1}·K^{-1}) and Gibbs free energies (ΔG, in kcal·mol^{-1}), computed at 80ºC and 1 atm in acetonitrile, of the stationary points involved in the 32CA reaction of nitrone **15** with allene **18**.

	H	ΔH	S	ΔS	G	ΔG
15	-558.023433		119.7		-558.090824	
18	-116.634245		63.2		-116.669808	
TS1	-674.611751	28.8	138.6	-44.3	-674.689757	44.5
TS2	-674.614645	27.0	138.8	-44.1	-674.692763	42.6
19	-674.678177	-12.9	137.1	-45.8	-674.755352	3.3
20	-674.690391	-20.5	137.1	-45.9	-674.767541	-4.3

[a] Relative to the separated reagents nitrone **15** and allene **18**.

The geometries in acetonitrile of the TSs involved in the 32CA reaction of nitrone **15** with the simplest allene **18** are given in Figure S1. At **TS1**, the distances between the C1 and C5 atoms, and the C4 and O3 atoms are 2.056 Å and 2.202 Å, while at **TS2** the distances between the O3 and C5 atoms, and the C1 and C4 atoms are 2.011 Å and 2.211 Å, respectively. Considering that the formation of the C−O bond takes place at a shorter distance than the C−C one, these lengths indicate that the more unfavourable **TS1** is more advanced than **TS2**. It is interesting to remark that along the two regioisomeric channels, the C1−C2 double bond framework of allene **18** approaches parallel to the molecular plane of nitrone **15**.

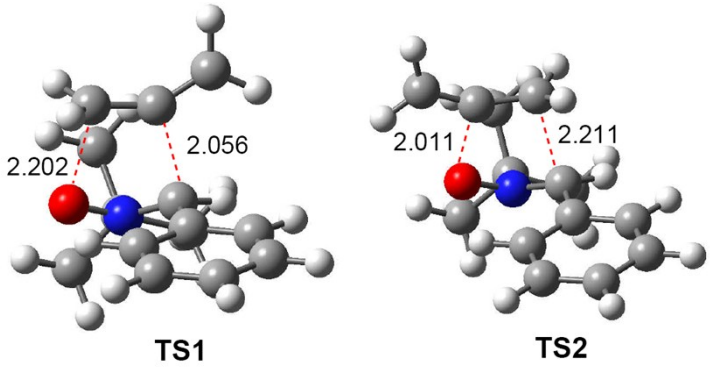

Figure S1. B3LYP/6-311G(d,p) geometries in acetonitrile of the TSs involved in the 32CA reaction of nitrone **15** with the simplest allene **18**. Distances are given in Angstroms, Å.

In order to evaluate the polar or non-polar electronic nature of these TSs, the global electron density transfer (GEDT)[1] was analysed by the sum of the natural atomic charges, obtained through a natural population analysis (NPA), of all the atoms belonging to either the allene or nitrone interacting fragments. The GEDT at the TSs involved in the 32CA reaction of nitrone **15** with the simplest allene **18** in acetonitrile is 0.00 e at **TS1** and 0.01 e at **TS2**. These negligible values indicate that this 32CA reaction has non-polar character, in clear agreement with the very high activation energy found in this 32CA reaction, and with the analysis of the conceptual DFT indices[2] at the ground state (GS) of the reagents.

*2. BET study of the regiosiomeric r1 reactive channel associated with the 32CA reaction between nitrone **15** and the simplest allene **18**.*

When trying to achieve a better understanding of bonding changes in organic reactions, the so-called BET[3] has proved to be a very useful methodological tool. This approach is used to understand the bonding changes along the reaction path and, consequently, to establish the nature of the electronic rearrangement associated with a given molecular mechanism.[4] In order to understand the different reactivity of nitrones towards linear or strained allenes, a BET study of the 32CA reaction of nitrone **15** with the simplest linear allene **18** yielding isoxazolidine **19** was first carried out in order to characterise its molecular mechanism.

BET study of the regiosiomeric *r1* reactive channel associated with the 32CA reaction between nitrone **15** and the simplest allene **18** indicates that this reaction can be topologically characterised by eight differentiated phases. The eight phases in which the reaction path is topologically divided are shown in Figure S2 on the representation of the relative energy for the cycloaddition process along the IRC. The populations of the most significant valence basins (those associated with the bonding regions directly involved in the reaction) of the selected points of the IRC are gathered in Table S2, the attractor positions of the ELF basins for the points involved in the bond formation processes are shown in Figure S3 and the basin-population changes along the reaction path are graphically represented in Figure S4.

The long *Phase I* (see Figure S2), 5.27 Å ≥ d(C1–C5) > 2.30 Å and 4.12 Å ≥ d(O3–C4) > 2.31 Å, starts at **MC1**, d(C1–C5) = 5.265 Å and d(O3–C4) = 4.120 Å, which is a minimum in the reaction path connecting the separated reagents, nitrone **15** and simplest allene **18**, with the TS of the reaction, **TS1**. The ELF picture of **MC1** usually shows the topological characteristics of the separated reagents. It may be seen two pairs of disynaptic basins, V(C4,C5) and V'(C4,C5), and V(C5,C6) and V'(C5,C6), integrating a total population of 3.72 e and 3.71 e, related with the two C1–C2 and C1–C6 double bonds of allene. On the other hand, two V(C1,N2) and V(N2,O3) disynaptic basins, presenting a population of 3.88 e and 1.36 e, and two V(O3) and V'(O3) monosynaptic basins, integrating a total population of 5.96 e, describe the C1–N2 double and the N2–O3 single bonds, and the O3 oxygen lone pairs of the nitrone fragment. Note that, according to the electron density values, the N2–O3 single

bond of the nitrone is strongly polarised towards the O3 oxygen of nitrone **15**. At **MC1**, the GEDT is null.

The very narrow *Phase II* (see Figure S2), 2.30 Å ≥ d(C1–C5) > 2.29 Å and 2.31 Å ≥ d(O3–C4) ≥ 2.30 Å, begins at **P1**. The most notable topological changes at this phase are the formation of one V(C1) monosynaptic basin with an initial population of 0.28 e, and a V(N2) monosynaptic basin, which integrates 0.83 e, both on the nitrone fragment, by means of a two concurrent fold $[F^{\dagger}]_2$ catastrophes. It is noteworthy that the V(C1) monosynaptic basin is related to a C1 *pseudoradical* center, while the V(N2) monosynaptic basin is related to the N2 nitrogen lone pair present at the final isoxazolidine **19**. Formation of both monosynaptic basins is a result of a depopulation of the V(C1,N2) disynaptic basin, which strongly decreases to 2.88 e. Note that until *Phase VI*, the GEDT is practically negligible.

Phase III, 2.29 Å ≥ d(C1–C5) > 2.12 Å and 2.30 Å ≥ d(O3–C4) > 2.22 Å, begins at **P2**. At this point, the most relevant topological change observed is the merger of the two V(C4,C5) and V'(C4,C5) disynaptic basins of the allene moiety into one new V(C4,C5) disynaptic basin, integrating 3.55 e, by a cusp *C* catastrophe. The population of the V(C1) and V(N2) monosynaptic basins have not been increased in this phase.

Phase IV, 2.12 Å ≥ d(C1–C5) > 1.91 Å and 2.22 Å ≥ d(O3–C4) > 2.11 Å, begins at **P3**. The most remarkable topological change at this phase is the formation of a new V(C5) monosynaptic basin on the central C5 carbon of the allene moiety with an initial population of 0.51 e by means of a fold $F^{\dagger}$ catastrophe. Note that while the V(C1) monosynaptic basin has reached a population of 0.44 e, the V(C4,C5) disynaptic basins suffers a strong depopulation by *ca.* 0.52 e. Additionally, the V(C1,N2) disynaptic basin also decreases its population to 2.50 e, whereas the population of V(N2) monosynaptic basin integrates 1.24 e. It is worth to mention that the two C1 and C5 *pseudoradical* centers are demanded for the subsequent C1–C5 single bond formation.[1] Within this phase, at d(C1–C5) = 2.070 Å and d(O3–C4) = 2.195 Å, the **TS1** of the reaction is found. Note that at **TS1**, the populations of the V(C1) and V(C5) monosynaptic basins have increased to 0.50 e and 0.60 e, respectively. The GEDT at **TS1** is 0.0 e.

The short *Phase V* (see Figure S2), 1.91 Å ≥ d(C1–C5) > 1.89 Å and 2.11 Å ≥ d(O3–C4) > 2.10 Å, begins at **P4** and it corresponds to a cusp ***C*** catastrophe. At this phase, one of the most significant topological changes along the reaction path takes place, consisting of the formation of one V(C1,C5) disynaptic basin by the merger of

the two V(C1) and V(C5) monosynaptic basins present in the previous phase, integrating a population of 1.44 e (see **P3** and **P4** in Figure S3, and the merger of V(C1) and V(C5), in green in **P3**, into V(C1,C5), in blue in **P4**, in Figure S4) .This relevant topological change indicates that the formation of the first C1–C5 single bond begins at a C1–C5 distance of 1.91 Å by a C-to-C coupling of two C1 and C5 *pseudoradical* centers.[1]

Phase VI, 1.89 Å ≥ d(C1–C5) > 1.60 Å and 2.10 Å ≥ d(O3–C4) > 1.80 Å, begins at **P5**. At this point, the most remarkable topological change is the formation of a new V(C4) monosynaptic basin on the allene moiety, integrating 0.13 e, by means of a fold $F^{\dagger}$ catastrophe. It is worth to note that at the end of this phase the population of the V(C4) monosynaptic basin reaches a value of 0.32 e (not shown in Table S2). No other relevant electron density changes are observed in this phase.

Phase VII, 1.60 Å ≥ d(C1–C5) > 1.59 Å and 1.80 Å ≥ d(O3–C4) > 1.76 Å, begins at **P6**. The most important topological change along this phase is associated to a fold *F* catastrophe consisting of the disappearance of the V(C4) monosynaptic basin created in the previous *Phase VI* (see **P6** in Figure S3). The ELF of the point of the IRC immediately before **P6** indicates that besides an electron density exchange between the V(O3) and V'(O3) monosynaptic basins, the electron density belonging to the disappeared V(C4) monosynaptic basin appears to be transferred to the V(O3) monosynaptic basins by means of the GEDT process, thus reaching a total population of 6.15 e. The population of the V(N2) monosynaptic basin has increased by 0.44 e as a result of the depopulation of the V(C1,N2) and V(N2,O3) disynaptic basins, which integrate 1.93 e and 1.01 e. Note that the increase of the population of the V(O3) monosynaptic basin, oriented towards the –Ph phenyl substituent of the nitrone framework (see Figure S3), is notably more pronounced than that of the V'(O3) monosynaptic one, whose population has slightly decreased. Besides, the population of the V(C1,C5) disynaptic basin integrates 1.88 e. At **P6**, the GEDT of the allene moiety is 0.23 e.

The last *phase VIII*, 1.59 Å ≥ d(C1–C5) > 1.53 Å and 1.76 Å ≥ d(O3–C4) > 1.44 Å, begins at **P7** and ends at isoxazolidine **19**. This point is characterised by a cusp $C^{\dagger}$ catastrophe consisting of the creation of a new V(O3,C4) disynaptic basin with an initial population of 0.76 e (see **P7** in Figure S3 and the creation of V(O3,C4), in blue in **P7**, in Figure S4). Note that the total population of the V(O3) and V'(O3) monosynaptic basins

has decreased by *ca.* 0.78 e. Interestingly, this decrease is mainly associated to the V(O3) monosynaptic basin (see Table S2 and Figure S4). This topological change reveals the formation of the second O3–C4 single bond, which begins at a O3–C4 distance of 1.76 Å by the donation of the electron density of one of the two O3 oxygen lone pairs of the nitrone framework to the C2 carbon atom of the allene fragment.[5] At **P7**, the GEDT from the allene moiety to the nitrone one increases to 0.25 e.

Finally, at isoxazolidine **19**, d(C1–C5) = 1.527 Å and d(O3–C4) = 1.438 Å, the two V(C1,C5) and V(O3,C4) disynaptic basins have reached populations of 1.99 e and 1.26 e, while the final populations of the V(C4,C5), V(N2,O3) and V(C1,N2) disynaptic basins are 2.05 e, 0.93 e and 1.87 e, and those of the V(N2), and V(O3) and V'(O3) monosynaptic basins are 2.31 e and 5.06 e, respectively.

Some appealing conclusions can be drawn from this BET study: i) the reaction begins with the rupture of the C1−N2 double bond of the nitrone framework in order to create the C1 *pseudoradical* center; ii) this electronic change demands a very high energy cost, 23.4 kcal·mol^{-1}; once the C1 *pseudoradical* center is formed, the subsequent rupture of the C4−C5 double bond of the simplest allene framework and creation of the C5 *pseudoradical* center demands a very low energy cost, 0.76 kcal·mol^{-1} (see Table S2); iii) consequently, the activation energy associated to this non-polar 32CA reaction can be mainly associated to the rupture of the C1−N2 double bond of nitrone **15**; iv) formation of the first C1–C5 single bond begins at a C1–C5 distance of 1.91 Å by a C-to-C coupling of two C1 and C5 *pseudoradical* centers; v) otherwise, formation of the second O3–C4 single bond begins at a O3–C4 distance of 1.76 Å by the donation of the electron density of one of the two O3 oxygen lone pairs of the nitrone framework to the C2 carbon atom of the allene fragment; vi) formation of the second O3–C4 single bond begins when the first C1–C5 single bond has reached 95% of its final electron density (see Table S2). Consequently, in spite of the low asynchronicity found at **TS1** (see Figure S1), the mechanism of this 32CA reaction can be classified as a *two-stage one-step* mechanism;[6] and finally vii) the bonding changes along the non-polar 32CA reaction between nitrone **15** and the simplest allene **18** are similar to those along the polar 32CA reactions of *C*-phenyl-*N*-methyl nitrone **21** with electron-deficient acrolein **22**.[5]

Table S2. Valence basin populations N calculated from the ELF of the IRC points, **P1** - **P7**, defining the eight phases characterising the molecular mechanism of the regioisomeric *r1* reactive channel associated with the 32CA reaction between nitrone **15** and allene **18**. The stationary points **MC1**, **TS1** and isoxazolidine **18** are also included. Distances are given in Å, GEDT values and electron populations in e, and relative energies with respect **MC1** in kcal·mol^{-1}.

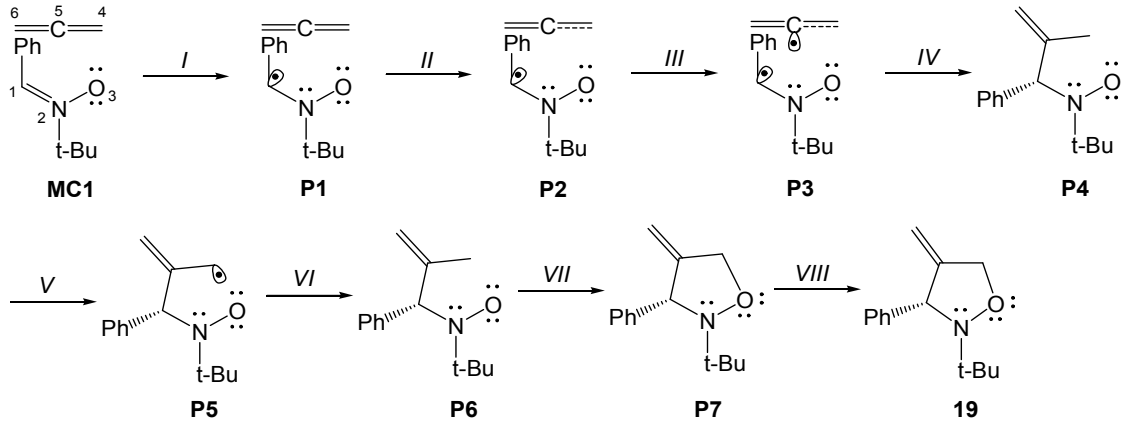

Points	15	18	MC1	P1	P2	P3	P4	P5	P6	P7	19	TS1
Catastrophes				$[F^{\dagger}]_2$	*C*	$F^{\dagger}$	*C*	$F^{\dagger}$	*F*	$C^{\dagger}$		
Phases			*I*	*II*	*III*	*IV*	*V*	*VI*	*VII*	*VIII*		
d(C1–C5)			5.265	2.297	2.292	2.122	1.909	1.885	1.601	1.586	1.527	2.070
d(O3–C4)			4.120	2.307	2.304	2.220	2.109	2.095	1.804	1.764	1.438	2.195
ΔE			0.0	23.4	23.5	26.7	24.4	23.6	4.1	1.7	-16.9	26.2
GEDT			0.00	-0.04	-0.04	-0.01	0.06	0.06	0.23	0.25	0.29	0.00
V(C1,N2)	3.81		3.88	2.88	2.89	2.50	2.21	2.17	1.93	1.94	1.87	2.41
V(N2)				0.83	0.83	1.24	1.66	1.72	2.16	2.17	2.31	1.36
V(N2,O3)	1.42		1.36	1.31	1.31	1.24	1.15	1.16	1.01	0.99	0.93	1.23
V(C4,C5)		1.84	1.84	1.86	3.55	3.03	2.61	2.54	2.20	2.17	2.05	2.92
V'(C4,C5)		1.85	1.88	1.72								
V(C5,C6)		1.84	1.85	1.87	1.88	1.87	1.86	1.85	1.81	1.83	1.78	1.88
V'(C5,C6)		1.85	1.86	1.82	1.83	1.80	1.75	1.75	1.76	1.75	1.76	1.77
V(C1)				0.28	0.28	0.44						0.50
V(C5)						0.51						0.60
V(O3)	2.99		3.03	2.90	2.90	2.91	2.82	2.85	3.39	2.68	2.51	2.86
V'(O3)	3.02		2.93	2.97	2.96	2.91	2.90	2.89	2.76	2.69	2.55	2.94
V(C4)								0.13				
V(C1,C5)							1.44	1.47	1.88	1.90	1.99	
V(O3,C4)										0.76	1.26	

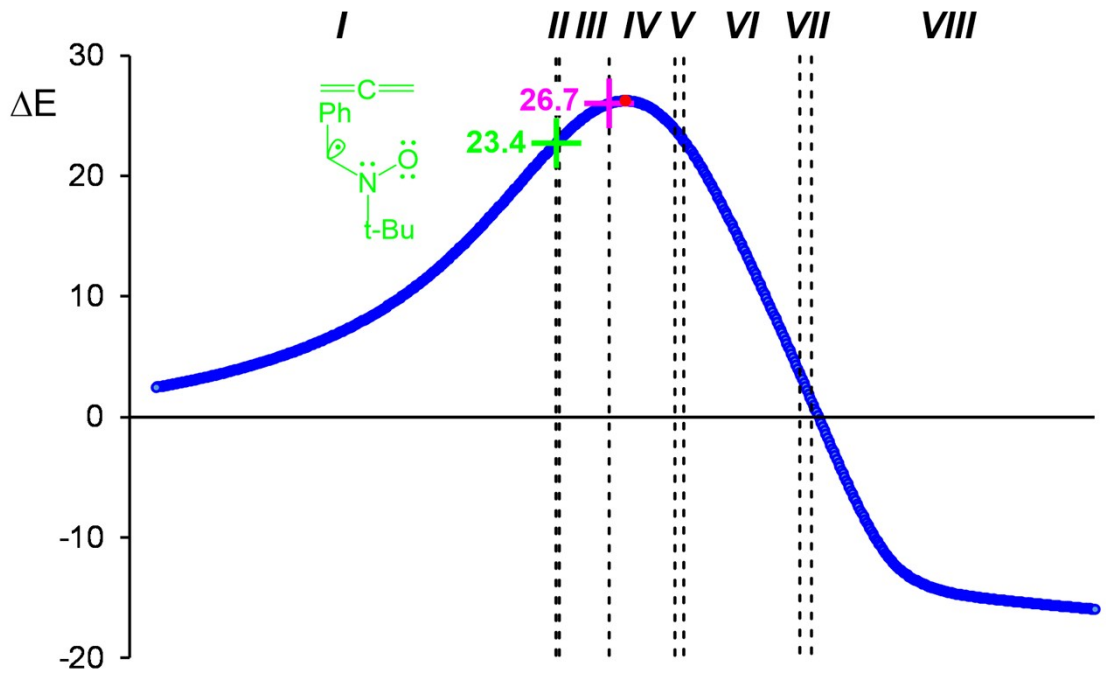

Figure S2. Relative energy (ΔE, in kcal·mol^{-1}) variations along the IRC (amu$^{1/2}$Bohr) associated with the regiosiomeric *r1* reactive channel of the 32CA reaction between nitrone **15** and the simplest allene **18**. Black hyphened lines separate the topological phases along the IRC, while the red point indicates the position of **TS1** and the green and magenta lines show the relative position of the points of the IRC associated with the formation of the C1 and C5 *pseudoradical* centers, respectively. Relative energies are given with respect to the separated reagents, while the energy costs are relative to **MC1**.

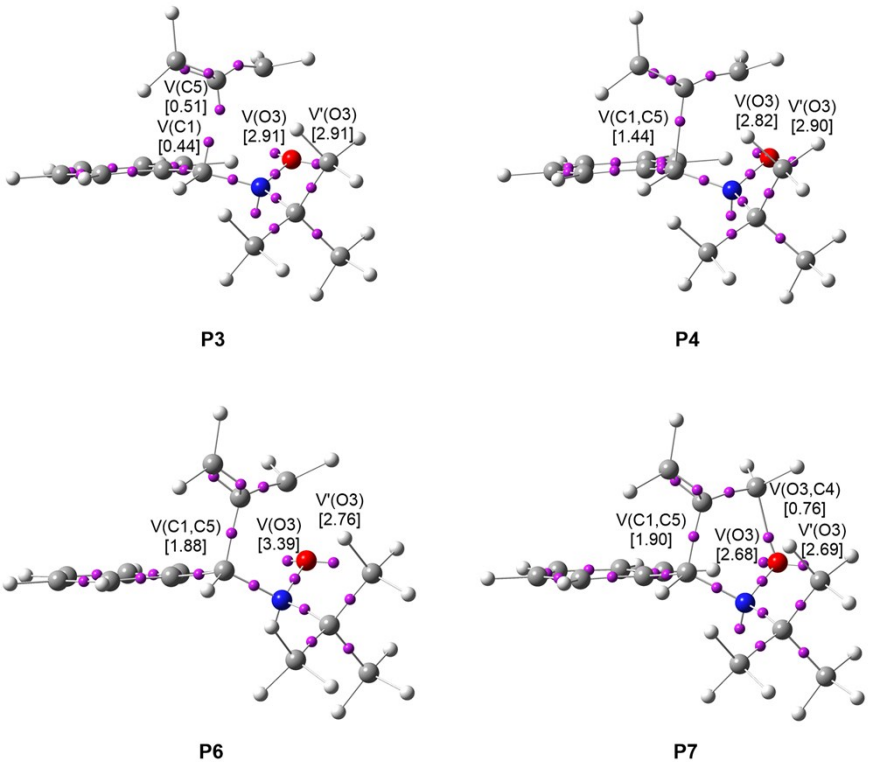

Figure S3. ELF attractor positions for the points of the IRC defining *Phases IV*, *V*, *VII* and *VIII* involved in the formation of the C1–C5 and O3–C4 single bonds along the regioisomeric *r1* reactive channel associated with the 32CA reaction between nitrone **15** and the simplest allene **18**. The electron populations, in e, are given in brackets.

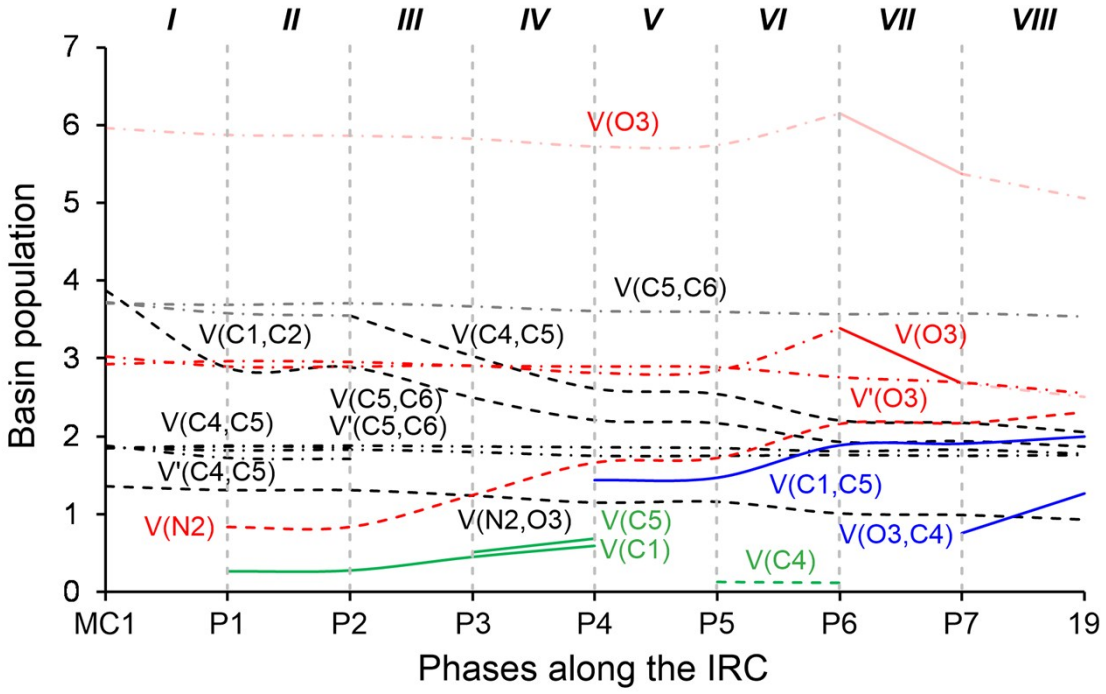

Figure S4. Graphical representation of the basin population changes along the regiosiomeric *r1* reactive channel associated with the 32CA reaction between nitrone **15** and the simplest allene **18**. Dash dotted curves represent bonding regions described by two basins, dashed curves represent bonding regions described by only one basin and lined curves represent the basins directly involved in the formation of the new single bonds; black curves represent basins that do not participate in the bond formation processes, grey curves represent the sum of basins characterising a bonding region, the red colour is for lone pairs, green for *pseudoradical* centers and blue for the new formed single bonds.

*3. BET study of the endo/ r1 reactive channel associated with the 32CA reaction between nitrone **15** and strained allene CHDE **10**.*

In order to understand the molecular mechanism of the 32CA reaction between nitrone **15** and strained allene CHDE **10**, a BET study of the most favourable *endo/r1* reaction channel was performed. This BET study indicates that this 32CA reaction takes place along ten differentiated phases related to the disappearance or creation of valence basins. The ten phases in which the reaction path is topologically divided are shown on the representation of the relative energy for the cycloaddition process along the IRC in Figure S5; separated by black hyphened lines crossing the energy curve. The populations of the most significant valence basins of the selected points of the IRC are included in Table S3, the attractor positions of the ELF basins for the points involved in the bond formation processes are shown in Figure S6 and the basin-population changes along the reaction path are graphically represented in Figure S7.

The very long *Phase I* (see Figure S5), 5.66 Å ≥ d(C1–C5) > 2.32 Å and 4.29 Å ≥ d(O3–C4) > 2.76 Å, begins at **MC1n**, which is a minimum in the PES connecting the separated reagents, nitrone **15** and strained allene CHDE **10**, with the TS of the reaction, **TS1n**. The electronic structure of MCs usually resembles that of the separated reagents (see Table S3). Thus, the allene framework of **MC1n** appears characterised by one V(C4,C5) disynaptic basin integrating 3.65 e, which is associated with the C4–C5 double bond of strained allene CHDE **10**, and two disynaptic basins, V(C5,C6) and V'(C5,C6), integrating a total of 3.76 e, related to the C5–C6 double bond. On the other hand, two V(C1,N2) and V(N2,O3) disynaptic basins, as well as two V(O3) and V'(O3) monosynaptic basins describe the C1–N2 double bond, the N2–O3 single bond and the O3 oxygen lone pairs of the nitrone moiety, with total electron populations of 3.87 e, 1.39 e and 5.94 e, respectively. These populations indicate that at **MC1n**, the N2–O3 single bond of the nitrone framework remains strongly polarised towards the O3 oxygen, a behaviour that will be maintained until the end of the reaction. At GEDT, the GEDT is null, 0.01 e.

The short *Phase II* (see Figure S5), 2.32 Å ≥ d(C1–C5) > 2.30 Å and 2.76 Å ≥ d(O3–C4) > 2.75 Å, begins at **P1n**, which corresponds to a $F^{\dagger}$ fold catastrophe implying the creation of a new V(C5) monosynaptic basin with an initial population of 0.41 e. This electron density, which is associated with a C5 *pseudoradical* center[1] at the strained allene framework, comes mainly from the depopulation of the V(C4,C5)

disynaptic basin by 0.36 e, while the V'(C5,C6) disynaptic basin has been slightly depopulated by 0.09 e. At the same time, the population of the V(C1,N2) disynaptic basin has slightly decreased to 3.83 e, as well as the total one of the V(O3) and V'(O3) monosynaptic basins to 5.88 e. From **MC1n** to **P1n**, the GEDT will approximately range in low values between ±0.04 e, which emphasises the non-polar character of this 32CA reaction.

The also narrow *Phase III* (see Figure S5), 2.30 Å ≥ d(C1–C5) > 2.25 Å and 2.75 Å ≥ d(O3–C4) > 2.74 Å, begins at **P2n**. At this point, together with the depopulation of the V(C1,N2) disynaptic basin by 0.26 e, a new V(C1) monosynaptic basin, related to the C1 *pseudoradical* center, is created at the C1 carbon of the nitrone framework with an initial population of 0.24 e, by means of another $F^{\dagger}$ fold catastrophe. Meanwhile, the V(C5) monosynaptic basin has reached a population of 0.46 e, at the same time that the V(C4,C5) disynaptic basins has slightly continued its depopulation to 3.26 e. Note that the two C1 and C5 *pseudoradical* centers are demanded for the C1–C5 single bond formation.[1]

Phase IV, 2.25 Å ≥ d(C1–C5) > 2.20 Å and 2.74 Å ≥ d(O3–C4) > 2.72 Å, begins at **P3n** and includes the TS of the reaction, **TS1n**, d(C1–C5) = 2.225 Å and d(O3–C4) = 2.726 Å. At **P3n**, the most notable topological change is the merger of the two V(C5,C6) and V'(C5,C6) disynaptic basins present at the previous phases into a new V(C5,C6) disynaptic basin (*C* cusp catastrophe) as a consequence of the slight depopulation of this bonding region by 0.07 e, while the V(C5) monosynaptic basin reaches a population of 0.55 e. At the other bonding regions, no relevant electron population variations are noticed. At **TS1n**, there are no significant population variations with respect to those described at **P3n**.

Phase V, 2.20 Å ≥ d(C1–C5) > 1.94 Å and 2.72 Å ≥ d(O3–C4) > 2.64 Å, begins at **P4n**. At this point, a new V(N2) monosynaptic basin has been created with an initial population of 0.80 e, simultaneously with the strong depopulation of the V(C1,N2) disynaptic basin to 2.82 e. This new V(N2) monosynaptic basin is related to the N2 nitrogen lone pair present at the final *endo* isoxazolidine **16a**. Parallel, while the V(C4,C5) disynaptic basin experiences a slight depopulation to 3.13 e, the V(C5) monosynaptic basin reaches a population of 0.65 e. Interestingly, the populations of the V(C4,C5) and V(C1,N2) disynaptic basins suggest that, according to Lewis's chemical bond model, the C1–C2 and N2–C5 double bonds of nitrone **15** and strained allene **10**

could be already partially broken at **P4**. On the other hand, the V(O3) and V'(O3) monosynaptic basins have maintained their populations practically invariable.

Phase VI, 1.94 Å ≥ d(C1–C5) > 1.59 Å and 2.64 Å ≥ d(O3–C4) > 2.42 Å, begins at **P5n**, which corresponds to a cusp *C* catastrophe. At this phase, the first most relevant topological change along the reaction path occurs; a new V(C1,C5) disynaptic basin is created by the merger of the two V(C1) and V(C5) monosynaptic basins present at the previous phase, with an initial population of 1.47 e (see **P4n** and **P5n** in Figure S6 and the merger of V(C1) and V(C5), in green in **P4n**, into the new V(C1,C5), in blue in **P5n**, in Figure S7). This relevant topological change indicates that the formation of the first C1–C5 single bond begins at a C1–C5 distance of 1.94 Å by a C-to-C coupling of two C1 and C5 *pseudoradical* centers.[1]

Phase VII, 1.59 Å ≥ d(C1–C5) > 1.56 Å and 2.42 Å ≥ d(O3–C4) > 2.25 Å, begins at **P6n**. At this point, while the V(C4,C5) disynaptic basin has been slightly depopulated by 0.06 e, a new V(C4) monosynaptic basin has been created with a population of 0.10 e, by means of a $F^{\dagger}$ fold catastrophe. The V(C1,N2) disynaptic basin has continued being considerably depopulated to 1.90 e, while the population of the V(C1,C5) disynaptic basin increases to 1.91 e. Note that at the beginning of this phase, the C1–C5 single bond has already reached 97% of its final population (see the evolution of the population of the V(C1,C5) disynaptic basin in Figure S7). The electron density lost by the V(C1,N2) disynaptic basin also contributes to the increase of the population of the V(N2) monosynaptic basin to 1.78 e, a value also achieved by the depopulation of the V(N2,O3) disynaptic basin by 0.07 e. At **P6n**, the GEDT taking place from the allene framework towards the nitrone one has increased to 0.10 e, as a consequence of a retro-donation process after the formation of the first C1–C5 single bond.

Phase VIII, 1.56 Å ≥ d(C1–C5) > 1.52 Å and 2.25 Å ≥ d(O3–C4) > 1.78 Å, begins at **P7n**. The most notable topological change taking place along this phase is the split of the V(C5,C6) disynaptic basin into two new V(C5,C6) and V'(C5,C6) disynaptic basins integrating 1.85 e and 1.55 e. This topological change, which is associated to a *C* cusp catastrophe, is just the consequence of an electron density redistribution within this bonding region, as its total population has only been increased by 0.01 e. Along this phase, other topological changes are observed, like the depopulation of the V(C4,C5) disynaptic basin to 2.48 e and the consequent population of the V(C4) monosynaptic to 0.27 e. Moreover, the V(N2) monosynaptic basin has

continued increasing its population until reaching 1.90 e, due to the depopulation of the V(C1,N2) disynaptic basin to 1.87 e, and accordingly, the population of the V(C1,C5) disynaptic basin has increased to 1.97 e. At **P7n**, the GEDT taking place from the allene framework towards the nitrone one is 0.14 e.

The extremely short *Phase IX* (see Figure S5), d(C1−C5) = 1.52 Å and 1.78 Å ≥ d(O3−C4) > 1.75 Å, begins at **P8n**. This point is characterised by a *F* fold catastrophe consisting of the disappearance of the V(C4) monosynaptic basin. Interestingly, besides an electron density exchange between the V(O3) and V'(O3) monosynaptic basins, topological analysis of the ELF of the point of the IRC immediately before **P8n** indicates that the electron density of the disappeared V(C4) monosynaptic basin has been redistributed within the V'(O3) monosynaptic one by means of the GEDT process, thus increasing its population by a total of 0.42 e (see V'(O3) in Figure S7). Note that this monosynaptic basin is that parallel oriented towards the Ph− phenyl substituent (see **P8n** in Figure S6). In addition, the total population of the V(C5,C6) and V'(C5,C6) disynaptic basins, as well as those of the V(N2) monosynaptic and V(C1,C5) disynaptic basins, have increased to 3.55 e, 2.21 e and 1.99 e, respectively, while the V(N2,O3) disynaptic basin has been depopulated to 0.97 e and the V(C1,N2) disynaptic basin has maintained its population. At **P8n**, the GEDT has strongly increased to 0.27 e. This high value is indicative of a high polarisation from the allene moiety towards the nitrone one before the formation of the second O3−C4 single bond.

Finally, *Phase X*, d(C1−C5) = 1.52 Å and 1.75 Å ≥ d(O3−C4) > 1.42 Å, begins at **P9n** and ends at *endo* isoxazolidine **16a**, d(C1−C5) = 1.522 Å and d(O3−C4) = 1.421 Å. At **P9n**, the second most significant topological change along the IRC path takes place by means of a $C^{\dagger}$ cusp catastrophe: while the V'(O3) monosynaptic basin has experienced a strong depopulation to 2.80 e, a new V(O3,C4) disynaptic basin has been created with an initial population of 0.61 e (see **P8n** and **P9n** in Figure S6 and the creation of the V(O3,C4), in blue in **P9n**, in Figure S7). This significant topological change indicates that the formation of the second O3−C4 single bond begins at a O3−C4 distance of 1.75 Å by the donation of the electron density of one of the nitrone O3 oxygen lone pairs to the C2 carbon atom of the allene framework. This pattern of formation of the O3−C4 is similar to that observed for the C−O single bond formation of the nitrone **21** with acrolein **22**.[5]

At *endo* isoxazolidine **16a**, only variations in electron populations with respect to those at **P9n** are observed. The two V(C1,C5) and V(O3,C4) disynaptic basins have reached populations of 1.97 e and 1.31 e, while the final populations of the V(C4,C5), V(N2,O3) and V(C1,N2) disynaptic basins are 2.07 e, 0.89 e and 1.87 e, and those of the V(N2), and V(O3) and V'(O3) monosynaptic basins are 2.37 e and 5.02 e.

Some appealing conclusions can be drawn from this BET study: i) the reaction begins with the rupture of the C4−C5 double bond of the strained cyclic allene framework in order to permit the creation of the C5 *pseudoradical* center. This electronic change demands a low energy cost, 8.3 kcal·mol^{-1}; ii) once the C5 *pseudoradical* center is formed in the strained cyclic allene framework, the subsequent rupture of the C1−N2 double bond of the nitrone fragment and creation of the C1 *pseudoradical* center has an unappreciable energy cost, 0.1 kcal·mol^{-1}. Consequently, once the C5 *pseudoradical* center is created, it induces the easy rupture of the C1−N2 double bond; iii) the low activation energy found in this non-polar 32CA reaction can be mainly associated to the fast creation of a *pseudoradical* species of strained allene CHDE **10**; iv) formation of the first C1–C5 single bond begins at a C1–C5 distance of 1.94 Å by a C-to-C coupling of two C1 and C5 *pseudoradical* centers.[1] Interestingly, the C5 *pseudoradical* centre participates with a high electron density, 0.89 e, to the formation of the new C1–C5 single bond; v) otherwise, formation of the second O3–C4 single bond begins at a O3–C4 distance of 1.75 Å by the donation of the electron density of one of the two O3 oxygen lone pairs of the nitrone framework to the C2 carbon atom of the allene fragment; vi) formation of the O3–C4 single bond takes place at the end of the reaction path once the first C1–C5 single bond has already reached 99% of its the population present at *endo* isoxazolidine **16a**. This fact allows characterising the molecular mechanism of this 32CA reaction as a non-concerted *two-stage one-step* mechanism.[6]

Table S3. Valence basin populations N calculated from the ELF of the IRC points, **P1 - P9**, defining the ten phases characterising the molecular mechanism of the most favourable reactive channel associated with the 32CA reaction between nitrone **15** and strained allene CHDE **10**. The stationary points **MC1n, TS1n** and *endo* isoxazolidine **16a** are also included. Distances are given in Å, GEDT values and electron populations in e, and relative energies with respect to **MC1n** in kcal·mol^{-1}.

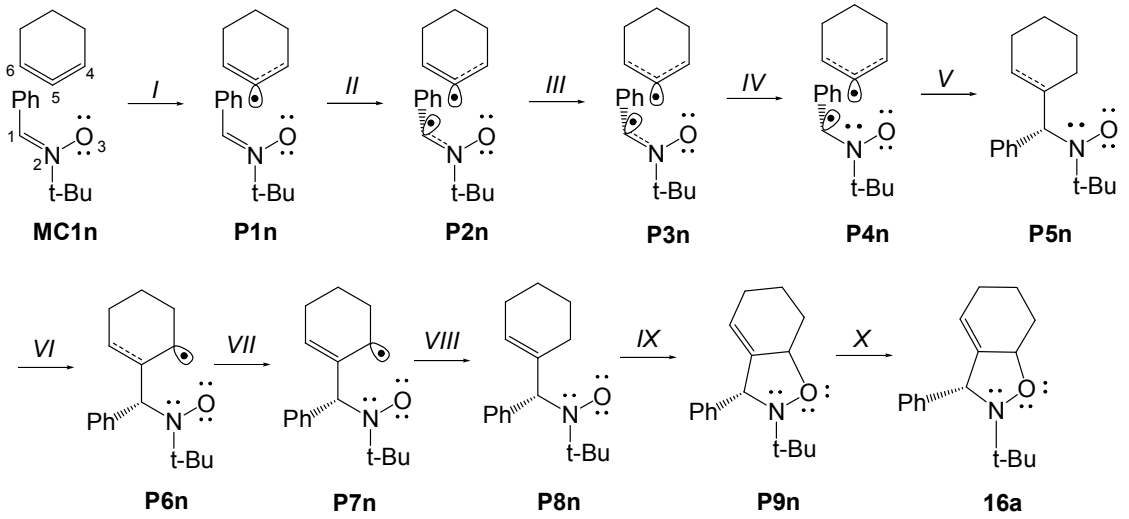

Points	15	10	MC1n	P1n	P2n	P3n	P4n	P5n	P6n	P7n	P8n	P9n	16a	TS1n
Catastrophes			*F*†		*F*†	*F*†	*C*	*C*	*F*†	*C*†	*F*	*C*†		
Phases			*I*	*II*	*III*	*IV*	*V*	*VI*	*VII*	*VIII*	*IX*	*X*		
d(C1−C5)			5.658	2.317	2.295	2.249	2.203	1.943	1.593	1.562	1.524	1.522	1.522	2.225
d(O3−C4)			4.290	2.762	2.753	2.737	2.720	2.641	2.424	2.252	1.779	1.752	1.421	2.726
ΔE			0.0	8.3	8.4	8.5	8.5	5.2	−7.9	−11.8	−29.3	−29.7	−51.6	8.5
GEDT			0.01	0.04	0.04	0.04	0.03	−0.01	−0.10	−0.14	−0.27	−0.28	−0.33	0.03
V(C1,N2)	3.81		3.87	3.83	3.60	3.61	2.82	2.28	1.90	1.87	1.85	1.85	1.87	3.61
V(N2)							0.80	1.36	1.78	1.90	2.21	2.21	2.37	
V(N2,O3)	1.42		1.39	1.35	1.33	1.33	1.33	1.27	1.20	1.14	0.97	0.95	0.89	1.33
V(C4,C5)		1.73	3.65	3.29	3.26	3.22	3.13	2.94	2.64	2.48	2.23	2.20	2.07	3.17
V'(C4,C5)		1.91												
V(C5,C6)		1.97	1.96	1.98	1.98	3.53	3.49	3.46	3.39	1.85	1.81	1.81	1.85	3.50
V'(C5,C6)		1.74	1.72	1.63	1.62					1.55	1.74	1.75	1.78	
V(C1)					0.24	0.29	0.33							0.32
V(C5)				0.41	0.46	0.55	0.65							0.61
V(O3)	2.99		3.01	3.02	2.87	2.97	2.98	2.94	2.91	2.97	2.79	2.75	2.48	2.97
V'(O3)	3.02		2.93	2.86	2.98	2.88	2.88	2.92	2.94	2.92	3.34	2.80	2.54	2.89
V(C4)									0.10	0.27				
V(C1,C5)								1.47	1.91	1.97	1.99	2.00	1.97	
V(O3,C4)												0.61	1.31	

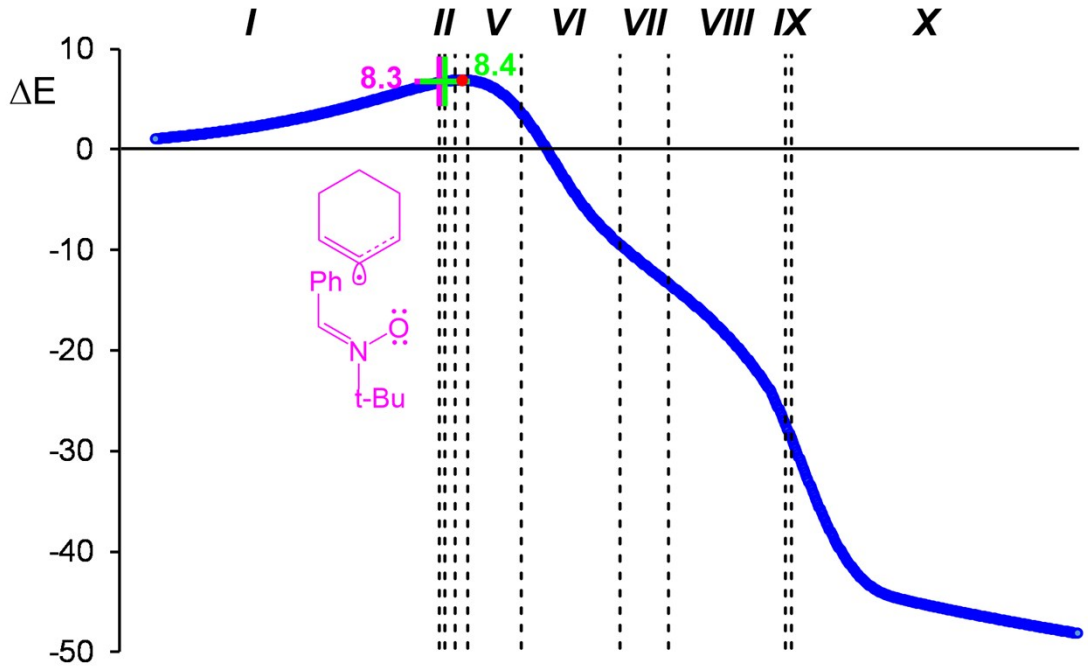

Figure S5. Relative energy (ΔE, in kcal·mol^{-1}) variations along the IRC (amu$^{1/2}$Bohr) associated with the most favourable *endo/r1* reactive channel of the 32CA reaction between nitrone **15** and strained allene CHDE **10**. Black hyphened lines separate the ten phases along the IRC, while the red point indicates the position of **TS1n** and the green and magenta lines show the relative position of the points of the IRC associated with the formation of the C1 and C5 *pseudoradical* centers, respectively. Relative energies are given with respect to the separated reagents, while the energy costs are relative to **MC1n**.

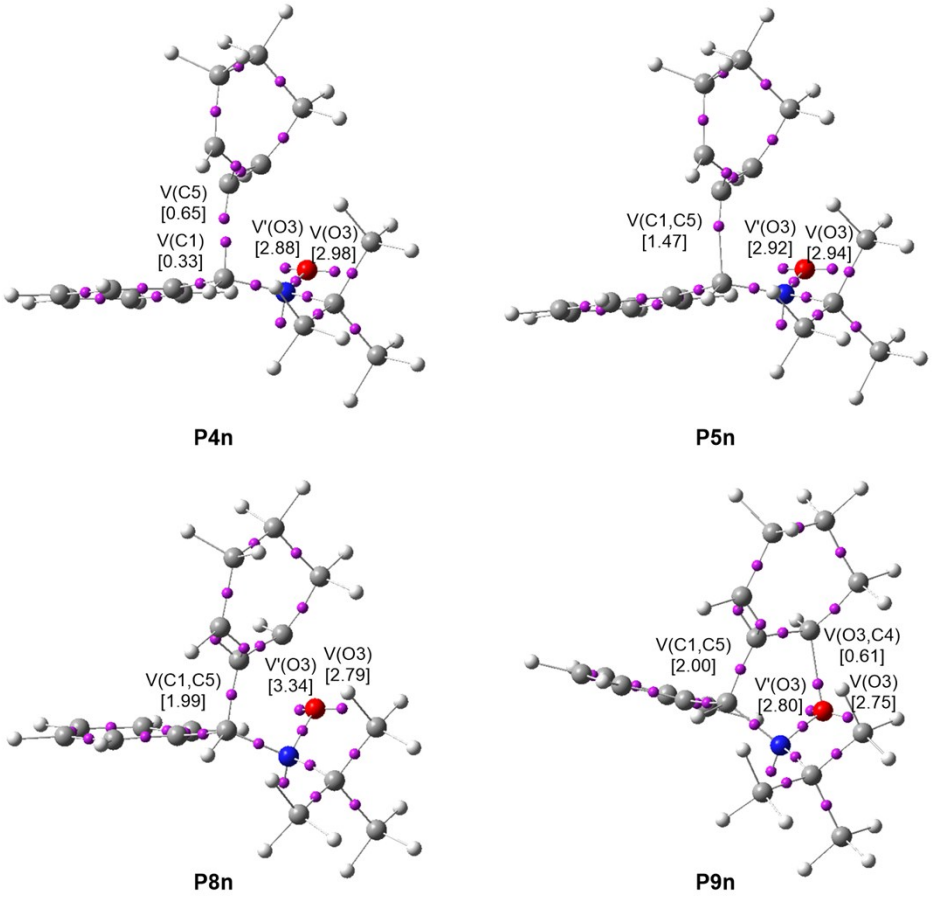

Figure S6. ELF attractor positions for the points of the IRC defining *Phases V*, *VI*, *IX* and *X* involved in the formation of the C1–C5 and O3–C4 single bonds along the most favourable *endo/r1* reactive channel associated with the 32CA reaction between nitrone **15** and strained allene CHDE **10**. The electron populations, in e, are given in brackets.

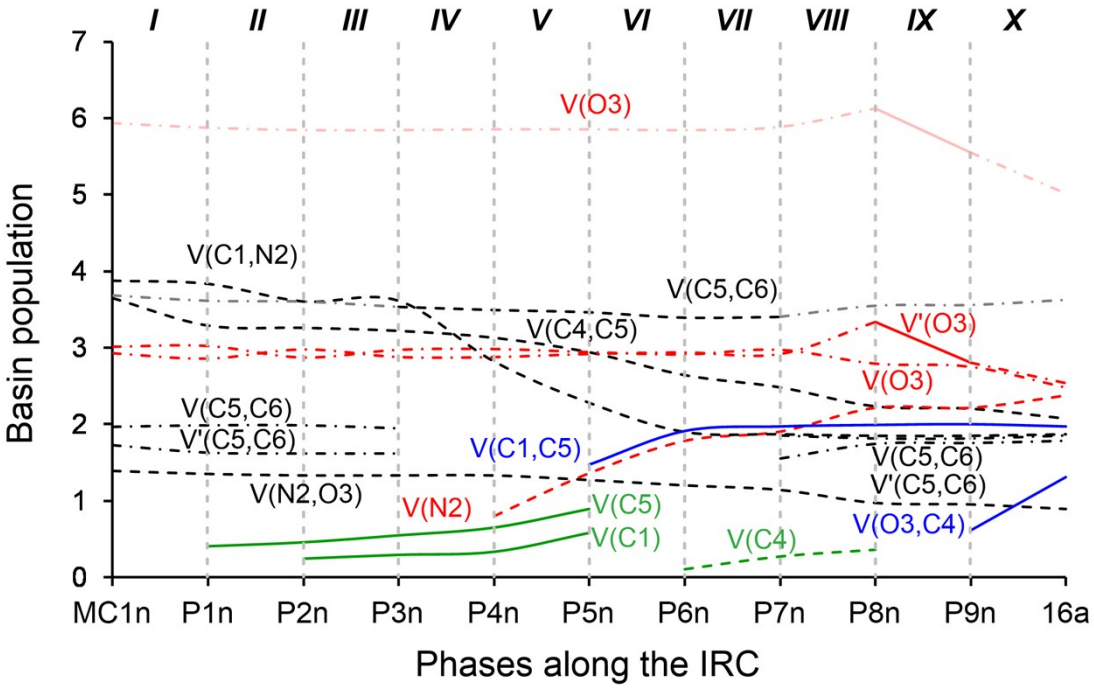

Figure S7. Graphical representation of the basin population changes along the most favourable *endo/r1* reactive channel associated with the 32CA reaction between nitrone **15** and strained allene CHDE **10**. Dash dotted curves represent bonding regions described by two basins, dashed curves represent bonding regions described by only one basin and lined curves represent the basins directly involved in the formation of the new single bonds; black curves represent basins that do not participate in the bond formation processes, grey curves represent the sum of basins characterising a bonding region, the red colour is for lone pairs, green for *pseudoradical* centers and blue for the new formed single bonds.

*4. ELF topological analysis along the exo/ r1 reactive channel associated with the 32CA reaction between nitrone **15** and strained allene CHDE **10**.*

Several theoretical studies devoted to the characterisation of the molecular mechanisms of *endo/exo* stereoisomeric reactive channels pairs have shown that they proceed through very similar molecular mechanisms. Thus, in order to characterise the molecular mechanism along the *exo/r1* reactive channel associated with the 32CA reaction between nitrone **15** and strained allene CHDE **10**, ELF topological analysis of the electronic structure of the corresponding TS, **TS1x**, and some representative points along the IRC was performed. The populations of the most significant valence basins are displayed in Table S4, while the attractor positions of the valence basins of the selected points of the IRC involved in the formation of the second O3–C4 single bond are represented in Figure S8.

At **TS1x**, d(C1–C5) = 2.137 Å and d(O3–C4) = 2.985 Å, a great similitude with respect to the topological features of **TS1n** is observed. Two V(C1) and V(C5) monosyanaptic basins, related to the two C1 and C5 *pseudoradical* centers demanded for the formation for the C1–C5 single bond, are present at **TS1x** with electron populations of 0.38 e and 0.49 e, respectively.

At **P1x**, d(C1–C5) = 1.567 Å and d(O3–C4) = 2.718 Å, which corresponds to the point where the *exo* IRC stops in gas phase, two V(N2) and V'(N2) monosynaptic basins integrating 0.62 e and 1.20 e describe the N2 nitrogen lone pair present at the final *exo* isoxazolidine **16b**. On the other hand, no V(C4) monosynaptic basin is yet observed as a consequence of the high O3–C4 distance at the *exo* **P1x**, 2.718 Å.

At **P2x**, d(C1–C5) = 1.533 Å and d(O3–C4) = 1.777 Å, one V(C4) monosynaptic basin associated with the C4 *pseudoradical* center, integrating 0.36 e, and only one V(N2) monosynaptic basin associated with the N2 lone pair, integrating 2.13 e, are observed. Interestingly, a slight electron density exchange between both V(O3) and V'(O3) monosynaptic basins associated to the two nitrone O3 oxygen lone pairs can be noticed, which corresponds to the bonding changes occurring along *Phase VIII* of the *endo* pathway.

At **P3x**, d(C1–C5) = 1.532 Å and d(O3–C4) = 1.752 Å, which is geometrically equivalent to the *endo* **P9n**, some different topological features are observed. While the V(C4) monosynaptic basin is still present with practically the same electron population than in the previous **P2x**, 0.37 e, a new third V''(O3) monosynaptic basin appears at the

O3 oxygen atom integrating 0.38 e. This electron density entirely comes from the depopulation of the V'(O3) monosynaptic basin by 0.34 e, which is responsible for the formation of the second O3–C4 single bond along the *endo* pathway (see above). In addition, the formation of the O3–C4 single bond has not yet begun at **P3x**, while the C1–C5 single bond is completely formed, permitting to characterise the molecular mechanism of the *exo* channel also as a *two-stage one-step* mechanism.[6]

Finally, at **P4x**, d(C1–C5) = 1.529 Å and d(O3–C4) = 1.703 Å, while the two V(C4) and V''(O3) monosynaptic basins present at the previous **P3x** have disappeared, a new V(O3,C4) disynaptic basin is observed with an electron population of 0.85 e. This relevant topological change indicates that the formation of the second O3–C4 single bond has already begun at a O3–C4 distance of *ca.* 1.70 e by the sharing of the electron density of two O3 and C4 *pseudoradical* centers (see Figure S8). This pattern for the formation of the second O3–C4 single bond is somewhat different to that found along the *endo* pathway (see above), in agreement with the differences between the IRC profiles associated with both stereoisomeric channels (see Figure S9).

Some appealing conclusions can be drawn from this comparative ELF topological analysis: i) the bonding changes are slightly more delayed along the *exo* stereoisomeric reactive channel; ii) as the *endo* channel, the *exo* stereoisomeric pathway also follows a *two-stage one-step* mechanism in which the formation of the second O3–C4 single bond takes place once the first C1–C5 one is completely formed: iii) formation of the first C1–C5 single bond takes place by the C-to-C coupling of two C1 and C5 *pseudoradical* centers, similarly to the *endo* channel; and finally, iv) formation of the second O3–C4 single bond takes place by the sharing of the electron density of two O3 and C4 *pseudoradical* centers. This bond formation pattern is somewhat different to that found along the *endo* channel, in which the electron density of the C4 *pseudoradical* center is redistributed into the O3 oxygen lone pairs resulting in the formation model by donation.

Table S4. Valence basin populations N calculated from the ELF of **TS1x** and the IRC points, **P1x** – **P4x**, of the *exo/r1* reactive channel associated with the 32CA reaction between nitrone **15** and strained allene CHDE **10**. Distances are given in Å, GEDT values and electron populations in e, and relative energies[a] in kcal·mol^{-1}.

Points	**TS1x**	**P1x**	**P2x**	**P3x**	**P4x**
d(C1–C5)	2.137	1.567	1.533	1.532	1.529
d(O3–C4)	2.985	2.718	1.777	1.752	1.703
ΔE	7.6	−5.1	−21.4	−22.4	−24.7
GEDT	0.03	−0.03	−0.25	−0.26	−0.27
V(C1,N2)	3.57	1.89	1.77	1.77	1.78
V(N2)		0.62	2.13	2.14	2.16
V’(N2)		1.20			
V(N2,O3)	1.35	1.26	0.99	0.97	0.94
V(C4,C5)	3.35	2.99	2.21	2.19	2.19
V’(C4,C5)					
V(C5,C6)	3.51	3.27	1.73	1.73	1.76
V’(C5,C6)			1.81	1.81	1.80
V(C1)	0.38				
V(C5)	0.49				
V(O3)	2.96	2.88	2.75	2.77	2.73
V’(O3)	2.92	2.92	3.04	2.70	2.70
V’’(O3)				0.38	
V(C4)			0.36	0.37	
V(C1,C5)		1.90	2.00	2.01	2.01
V(O3,C4)					0.85

[a] Relative to the separated reagents CHDE **10** and nitrone **15**.

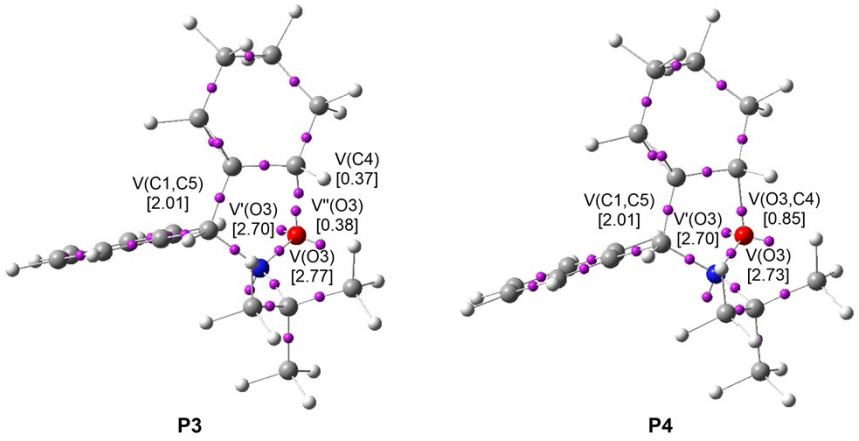

Figure S8. ELF attractor positions for the selected points of the IRC involved in the formation of the second O3–C4 single bond, **P3x** and **P4x**, along the *exo/r1* reactive channel associated with the 32CA reaction between nitrone **15** and strained allene CHDE **10**. The electron populations, in e, are given in brackets.

4. Theoretical background

4.1 Topological analysis of the electron localisation function (ELF)

Like many other chemical concepts, chemical bonds are defined in a rather ambiguous manner as they are not observable, but rather belong to a representation of the matter at a microscopic level, which is not fully consistent with quantum mechanical principles. To harmonise the chemical description of matter with quantum chemical postulates, several mathematical models have been developed. Among them, the theory of dynamical systems,[7] convincingly introduced by Bader through the Theory of Atoms in Molecules (AIM),[8] has become a powerful method of analysis. The AIM theory enables a partition of the electron density within the molecular space into basins associated with atoms. Another appealing procedure that provides a more straightforward connection between the electron density distribution and the chemical structure is the quantum chemical analysis of the ELF of Becke and Edgecombe.[9] ELF constitutes a useful relative measure of the electron pair localisation characterising the corresponding electron density.[10] Within the framework of Density Functional Theory (DFT), ELF is a density-based property that can be interpreted in terms of the positive-definite local Pauli and Thomas Fermi kinetic energy densities in a given system. In the validity of such a framework, these quantities provide key information to evaluate the relative local excess of kinetic energy density associated to the Pauli principle. ELF presents values in the range [0,1]; the highest values being associated with the spatial positions with higher relative electron localisation.[9-11] After an analysis of the electron density, ELF provides basins of attractors, which are the domains in which the probability of finding an electron pair is maximal. The spatial points in which the gradient of ELF has a maximum value are designated as attractors.[12] ELF basins are classified as core basins, C(...), and valence basins, V(...). The latter are characterised by the synaptic order, *i.e.* the number of atomic valence shells in which they participate. Thus, there are monosynaptic, disynaptic, trisynaptic basins and so on.[13] Monosynaptic basins, labelled V(A), correspond to the lone pairs or non-bonding regions, while disynaptic basins, labelled V(A,B), connect the core of two nuclei A and B and, thus, correspond to a bonding region between A and B. This description recovers the Lewis bonding model, providing a very suggestive graphical representation of the molecular system.

4.2 Bonding Evolution Theory (BET)

When trying to achieve a better understanding of bonding changes in organic chemical reactions, the so-called BET has proved to be a very useful methodological tool.[3] BET applies Thom's Catastrophe Theory (CT) concepts[14] to the topological analysis of the gradient field of the ELF.[9]

Within the BET methodology,[3] the structural stability of the critical points of the ELF gradient field is examined for the system of nuclei and electrons 'evolving' along the Born-Oppenheimer energy hypersurface or a given reduced reaction coordinate, *e.g.* the intrinsic reaction coordinate, occurring as a result of the variation in the control space parameters from reactive to product configurations. The chemical process becomes thus rationalised in terms of successive structural stability domains (SSDs), also called phases, comprising structures along the path where the number and type, *e.g.* synaptic orders, of critical points of the gradient field of ELF remain without changes.[3]

Within the BET context, the turning points between these phases are located and the discontinuities or bifurcation catastrophes can be identified. BET allows, thus, characterising unequivocally the behaviour of the dynamical system upon bifurcations associated with the ELF gradient field changing along the reaction coordinate. The different catastrophes in this case correspond to the reduction or the increase of the critical points associated with attractors of electron pairs defining bonding and non-bonding, *e.g.* lone pairs, domains for electron (de)localisation.

A detailed examination of the topology of ELF along the Intrinsic Reaction Coordinate (IRC) pathway for a given reaction reveals the existence of several catastrophes belonging exclusively to the fold, F and $F^{\dagger}$, and cusp, C and $C^{\dagger}$, elementary types, according to Thom's classification. The F catastrophe merges an attractor and a saddle point into a wandering point, *i.e.* a non-critical point, decreasing the number of basins by 1, whereas $F^{\dagger}$ splits a wandering point into an attractor and a saddle point increasing the number of basins by 1. The $\dagger$ superscript is utilised in those catastrophes where either the number of attractors or the synaptic order increase. The cusp catastrophe C merges two attractors and a saddle point into an attractor decreasing the number of basins by 1, while $C^{\dagger}$ splits an attractor into two attractors and a saddle point increasing the number of basins by 1. The symbol of a catastrophe written in bold is used to mark a catastrophe leading to the formation of the first covalent bond. The analysis of the changes in the number and type of ELF valence basins for the structures

involved along the IRC of the reaction allows establishing a set of points, **Pi**, separating the different phases that characterise the studied molecular mechanism.

Several theoretical studies have shown that the topological analysis of the ELF offers a suitable framework for the study of the changes of electron density.[15] This methodological approach is used as a valuable tool to understand the bonding changes along the reaction path and, consequently, to establish the nature of the electronic rearrangement associated with a given molecular mechanism within a BET perspective.

References

1 L. R. Domingo, *RSC Adv.*, 2014, **4**, 32415-32428.

2 (a) P. Geerlings, F. De Proft and W. Langenaeker, *Chem. Rev.*, 2003, **103**, 1793-1873; (b) L. R. Domingo, M. Ríos-Gutiérrez and P. Pérez, *Molecules*, 2016, **21**, 748.

3 X. Krokidis, S. Noury and B. Silvi, *J. Phys. Chem. A* 1997, **101**, 7277−7282.

4 (a) S. Berski, J. Andrés B. Silvi and L. R. Domingo, *J. Phys. Chem. A* 2003, **107**, 6014–6024; (b) S. Berski, J. Andrés, B. Silvi and L. R. Domingo, *J. Phys. Chem. A.* 2006, **110**, 13939–13947; (c) V. Polo, J. Andrés, S. Berski, L. R. Domingo and B. Silvi, *J. Phys. Chem. A* 2008, **112**, 7128–7134; (d) J. Andrés, P. González-Navarrete and V. S. Safont, *Int. J. Quant. Chem.* 2014, **114**, 1239–1252; (e) J. Andrés, S. Berski, L. R. Domingo, V.Polo and B.Silvi, *Curr. Org. Chem.* 2011, **15**, 3566–3575; (f) J. Andrés, L. Gracia, P. González-Navarrete and V. S. Safont, *Comp. Theor. Chem.* 2015, **1053**, 17–30.

5 M. Ríos-Gutiérrez, P. Pérez and L. R. Domingo, RSC Adv., 2015, **5**, 58464–58477.

6 L. R. Domingo, J. A. Saéz, R. J. Zaragozá and M. Arnó, *J. Org. Chem.*, 2008, **73**, 8791–8799.

7 R. H. Abraham and C. D. Shaw, *Dynamics: The Geometry of Behavior*, Addison-Wesley, Redwood City, CA, 1992.

8 R. F. W. Bader, *Atoms in Molecules. A Quantum Theory*, Claredon Press, Oxford, U.K, 1990.

9 A. D. Beck and K. E. Edgecombe, *J. Chem. Phys.* 1990, **92**, 5397–5403.

10 (a) B. Silvi and A. Savin, *Nature* 1994, **371**, 683−686; (b) A. Savin, B. Silvi, and F. Colonna, *Can. J. Chem.* 1996, **74**, 1088–1096.

11 (a) A. Savin, A. D. Becke, J. Flad, R. Nesper, H. Preuss and H. G. Vonschnering, *Angew. Chem. Int. Ed.* 1991, **30**, 409–412: (b) A. Savin, R. Nesper, S. Wengert and T. F. Fassler, *Angew. Chem. Int. Ed.* 1997, **36**, 1809–1832.

12 A. Savin, *J. Chem. Sci.* 2005, **117**, 473–475.

13 B. Silvi, *J. Mol. Struct.* 2002, **614**, 3–10.

14 (a) R. Thom, *Structural Stability and Morphogenesis: An Outline of a General Theory of Models*, Inc., Reading, Mass (London-Amsterdam, 1976); (b) A. E. R. Woodcock and T. Poston, *A Geometrical Study of Elementary Catastrophes,* (Spinger-Verlag, Berlin, 1974); (c) R. Gilmore, *Catastrophe Theory for Scientists and Engineers* (Dover, New York, 1981).

15 (a) E. Chamorro, P. Fuentealba and A. Savin, *J. Comput. Chem*. 2003, **24**, 496–504; (b) E. Chamorro, *J. Chem. Phys.* 2003, **118**, 8687–8698; (c) E. Chamorro, R. Notario, J. C. Santos and P. Pérez, *Chem. Phys. Lett.* 2007, **443**, 136–140; (d) L. R. Domingo, E. Chamorro and P. Pérez, *J. Org. Chem.* 2008, **73**, 4615–4624; (e) L. R. Domingo, E. Chamorro and P. Pérez, *Org. Biomol. Chem.* 2010, **8**, 5495–5504; (f) S. Berski and Z. Ciunik, *Mol. Phys.* 2015, **113**, 765–781; (g) M. Ríos-Gutiérrez, P. Pérez and L. R. Domingo, *RSC Adv.* 2015, **5**, 58464–58477.

Table S5. B3LYP/6-311G(d,p) enthalpies (H, in au), entropies (S, in cal·mol^{-1}·K^{-1}) and Gibbs free energies (G, in au); and relative[a] enthalpies (ΔH, in kcal·mol^{-1}), entropies (ΔS, in cal·mol^{-1}·K^{-1}) and Gibbs free energies (ΔG, in kcal·mol^{-1}) , computed at 80ºC and 1 atm in acetonitrile, of the stationary points involved in the 32CA reaction of nitrone **15** with CHDE **10**.

	H	ΔH	S	ΔS	G	ΔG
10	-233.285394		78.236		-233.329405	
15	-558.020445		122.092		-558.089127	
TS1n	-791.294681	7.0	155.732	−44.6	-791.382287	22.7
TS1x	-791.293487	7.8	156.499	−43.8	-791.381525	23.2
TS2n	-791.290883	9.4	154.749	−45.6	-791.377936	25.5
TS2x	-791.293587	7.7	154.955	−45.4	-791.380755	23.7
16a	-791.384151	−49.1	148.566	−51.8	-791.467725	−30.9
16b	-791.370464	−40.6	148.792	−51.5	-791.454165	−22.4
17a	-791.383801	−48.9	149.039	−51.3	-791.467641	−30.8
17b	-791.381446	−47.4	147.662	−52.7	-791.464512	−28.9

[a] Relative to the separated reagents CHDE **10** and nitrone **15**

*5. Analysis of the dependence of the thermodynamic data associated with the 32CA reaction between nitrone **15** and CHDE **10** with the DFT functional*

In order to check the thermodynamic data obtained by using the B3LYP/6-311G(d,p) level, the enthalpies, entropies and Gibbs free energies were computed performing thermodynamic calculations using the MPWB1K, ωB97XD and M06-2X functionals together with the 6-311G(d,p) basis set over the optimised B3LYP/6-311G(d,p) geometries in acetonitrile. The thermodynamic data obtained by using the four functionals are given in Tables S5-S8.

Analysis of the relative thermodynamic data makes it possible to obtain the following appealing conclusions: i) the computed TΔS values for the most favourable **TS1n** are found in a narrow range: 15.7 (B3LYP), 16.4 (MPWB1K), 15.9 (ωB97XD) and 15.6 (M06-2X) kcal·mol^{-1}. Consequently, the different relative Gibbs free energies obtained with the four functionals are mainly due to the computed relative enthalpies; ii) the activation enthalpies associated with **TS1n** are: 7.0 (B3LYP), 4.2 (MPWB1K), 0.1 (ωB97XD) and 0.0 (M06-2X) kcal·mol^{-1}. A similar trend was found for the activation energies associated to the non-polar Diels-Alder reaction between butadiene and ethylene, for which experimental data can be found. Comparing the four functionals, ωB97XD and M06-2X clearly underestimate activation enthalpies; iii) the reaction enthalpies associated with the formation of **16a** are: −49.1 (B3LYP), −67.5 (MPWB1K), −67.8 (wB97XD) and −68.9 (M06-2X) kcal·mol^{-1}. While B3LYP underestimates the reaction enthalpy, the other three functionals give similar values; iv) the four functionals give a low *endo* stereoselectivity, between 0.8 and 1.8 kcal·mol^{-1}; v) the B3LYP functional gives a poor regioselectivity, 0.7 kcal·mol^{-1}, while the MPWB1K and M06-2X give an inverse regioselectivity. Only the ωB97XD functional gives a high regioselectivity, 3.2 kcal·mol^{-1}, in clear agreement with the experimental results; vi) since the four functionals indicate that this 32CA reactions is irreversible, $\Delta G_{reac} < -18.1$ kcal·mol^{-1}, formation of **16a** and **16b** takes place *via* kinetic control. Consequently, this comparative analysis indicates that the B3LYP and MPWB1K functionals are the most adequate ones to study this non-polar 32CA reaction.

Full MPWB1K/6-311G(d,p) optimisations of **TS1n** and **TS1x** give more synchronous geometries than the B3LYP/6-311G(d,p) ones (see Figure S9). At the most

favourable **TS1n**, the C–O distance, 2.501 Å, becomes shorter than that found at B3LYP/6-311G(d,p), 2.726 Å. Interestingly, the highly asynchronous B3LYP/6-311G(d,p) **TS1x** becomes more synchronous at the MPWB1K/6-311G(d,p) level. The MPWB1K C–C and C–O distances, 2.265 and 2.336 Å, exclude the existence of any intermediate, asserting the one-step mechanism found at the B3LYP/6-311G(d,p) level along the *exo* stereoisomeric reaction channel, thus rejecting the stepwise mechanism found by Houk.

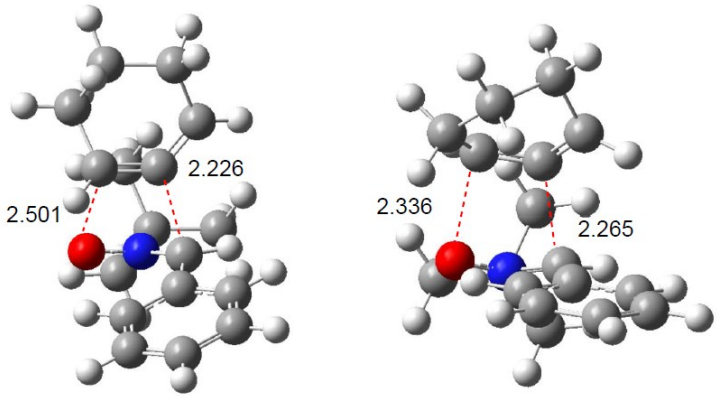

Figure S9. MPWB1K/6-311G(d,p) geometries of the **TS1n** and **TS1x** involved in the 32CA reaction of nitrone **15** with CHDE **10**. Distances are given in Angstroms, Å.

Table S6. MPWB1K/6-311G(d,p)//B3LYP/6-311G(d,p) enthalpies (H, in au), entropies (S, in cal·mol^{-1}·K^{-1}) and Gibbs free energies (G, in au); and relative[a] enthalpies (ΔH, in kcal·mol^{-1}), entropies (ΔS, in cal·mol^{-1}·K^{-1}) and Gibbs free energies (ΔG, in kcal·mol^{-1}), computed at 80ºC and 1 atm in acetonitrile, of the stationary points involved in the 32CA reaction of nitrone **15** with CHDE **10**.

	H	ΔH	S	ΔS	G	ΔG
10	-233.138502		76.429		-233.181497	
15	-557.698946		113.309		-557.762687	
TS1n	-790.830734	4.2	143.320	-46.4	-790.911357	20.6
TS1x	-790.828629	5.5	144.281	-45.5	-790.909793	21.6
TS2n	-790.828249	5.8	142.877	-46.9	-790.908623	22.3
TS2x	-790.831325	3.8	143.601	-46.1	-790.912107	20.1
16a	-790.944946	-67.5	137.181	-52.6	-791.022116	-48.9
16b	-790.932258	-59.5	137.990	-51.7	-791.009883	-41.2
17a	-790.945064	-67.5	137.659	-52.1	-791.022503	-49.1
17b	-790.944327	-67.1	138.392	-51.3	-791.022178	-48.9

[a] Relative to the separated reagents CHDE **10** and nitrone **15**.

Table S7. ωB97XD/6-311G(d,p)//B3LYP/6-311G(d,p) enthalpies (H, in au), entropies (S, in cal·mol^{-1}·K^{-1}) and Gibbs free energies (G, in au); and relative[a] enthalpies (ΔH, in kcal·mol^{-1}), entropies (ΔS, in cal·mol^{-1}·K^{-1}) and Gibbs free energies (ΔG, in kcal·mol^{-1}) , computed at 80ºC and 1 atm in acetonitrile, of the stationary points involved in the 32CA reaction of nitrone **15** with CHDE **10**.

	H	ΔH	S	ΔS	G	ΔG
10	-233.198950		77.740		-233.242682	
15	-557.826563		119.467		-557.893768	
TS1n	-791.025382	0.1	152.148	-45.1	-791.110972	16.0
TS1x	-791.022394	2.0	152.084	-45.1	-791.107948	17.9
TS2n	-791.020315	3.3	150.354	-46.9	-791.104896	19.8
TS2x	-791.025494	3.3	152.105	-46.9	-791.111060	19.8
16a	-791.133595	-67.8	145.245	-52.0	-791.215301	-49.5
16b	-791.122302	-60.7	146.204	-51.0	-791.204548	-42.7
17a	-791.134782	-68.6	145.339	-51.9	-791.216542	-50.3
17b	-791.133805	-68.0	145.590	-51.6	-791.215706	-49.7

[a] Relative to the separated reagents CHDE **10** and nitrone **15**.

Table S8. M06-2X /6-311G(d,p)//B3LYP/6-311G(d,p) enthalpies (H, in au), entropies (S, in cal·mol^{-1}·K^{-1}) and Gibbs free energies (G, in au); and relative[a] enthalpies (ΔH, in kcal·mol^{-1}), entropies (ΔS, in cal·mol^{-1}·K^{-1}) and Gibbs free energies (ΔG, in kcal·mol^{-1}) , computed at 80ºC and 1 atm in acetonitrile, of the stationary points involved in the 32CA reaction of nitrone **15** with CHDE **10**.

	H	ΔH	S	ΔS	G	ΔG
10	-233.167379		77.776		-233.242682	
15	-557.761592		117.913		-557.893768	
TS1n	-790.928900	0.0	151.664	-44.0	-791.110972	15.6
TS1x	-790.926347	1.6	152.959	-42.7	-791.107948	16.7
TS2n	-790.926791	1.4	151.273	-44.4	-791.104896	17.0
TS2x	-790.931705	-1.7	146.484	-49.2	-791.111060	15.6
16a	-791.038696	-68.9	145.105	-50,6	-791.215301	-51.0
16b	-791.026939	-61.5	147.119	-48,6	-791.204548	-44.3
17a	-791.039008	-69.1	146.159	-49.5	-791.216542	-51.6
17b	-791.038078	-68.5	145.691	-50.0	-791.215706	-50.8

[a] Relative to the separated reagents CHDE **10** and nitrone **15**.

Table S9. B3LYP/6-311G(d,p) total (E, in a.u.) and relative[a] energies (ΔE, in kcal·mol^{-1}), in gas phase and in acetonitrile, of the stationary points involved in the 32CA reaction of nitrone **15** with CHDE **10**.

	Gas phase		*Acetonitrile*	
	E	ΔE	E	ΔE
10	-233.411862		-233.414324	
15	-558.272170		-558.277230	
TS1n	-791.673213	6.8	-791.681419	6.4
TS1x	-791.671952	7.6	-791.680158	7.2
TS2n	-791.668947	9.5	-791.677247	9.0
TS2x	-791.672457	7.3	-791.679910	7.3
16a	-791.768900	-53.3	-791.774759	-52.2
16b	-791.756042	-45.2	-791.761112	-43.6
17a	-791.767237	-52.2	-791.774353	-52.0
17b	-791.765956	-51.4	-791.772262	-50.6

[a] Relative to the separated reagents CHDE **10** and nitrone **15**.

Table S10. B3LYP/6-311G(d,p) total (E, in a.u.) and relative[a] (ΔE, kcal·mol^{-1}), in gas phase and in acetonitrile, energies of the stationary points involved in the 32CA reaction of nitrone **15** with the simplest allene **18**.

	Gas phase		*Acetonitrile*	
	E	ΔE	E	ΔE
15	-558.272170		-558.280418	
18	-116.693199		-116.695021	
TS1	-674.923690	26.2	-674.930548	28.2
TS2	-674.926378	24.5	-674.933271	26.5
19	-674.993440	-17.6	-675.000566	-15.8
20	-675.005697	-25.3	-675.012819	-23.5

[a] Relative to the separated reagents linear allene **18** and nitrone **15**.

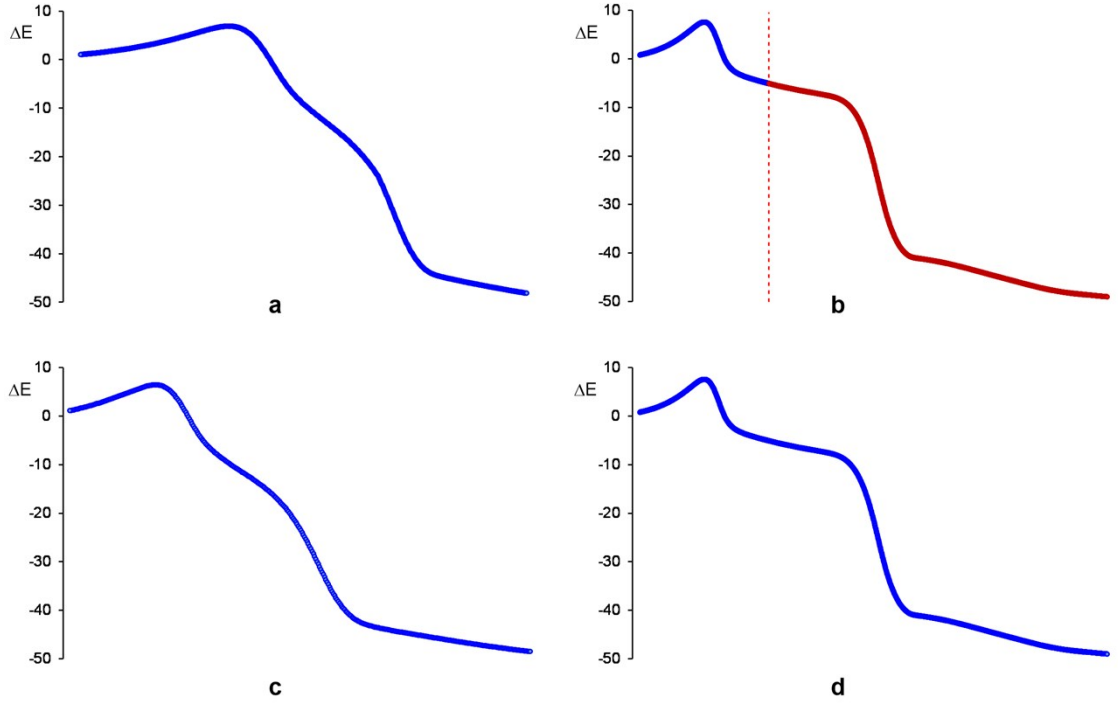

Figure S10. Relative energy (ΔE, in kcal·mol^{-1}) variations along the IRC (amu$^{1/2}$Bohr) associated with the *endo/r1* (a, c) and *exo/r1* (b, d) reactive channels of the 32CA reaction between nitrone **15** and strained allene CHDE **10**, in gas phase (a, b) and in acetonitrile (c, d). In the gas phase *exo/r1* profile (b) dashed red line in b indicates the point where the IRC stopes, while the reed curve corresponds to the IRC downhill calculations. Relative energies are given with respect to the separated reagents.

B3LYP/6-311G(d,p) computed total energies, only imaginary frequencies and Cartesian coordinates, in acetonitrile, of the structures involved in the 32CA reaction between nitrone **15** and strained allene CHDE **10**.

10
E(RB3LYP) = -233.414324 a.u.

C	-0.06312300	1.31650000	-0.16410400
C	1.32272600	0.58293300	-0.16008100
C	1.17458200	-0.89409800	0.22097000
C	-0.00353900	-1.39997900	-0.08950600
C	-1.19282600	-0.85637800	-0.27212800
C	-1.26285200	0.49805300	0.42547300
H	1.81750800	0.72426600	-1.12538100
H	1.90904800	-1.35761800	0.87091800
H	-1.90884600	-1.13687200	-1.03743800
H	-1.15754500	0.39887100	1.50803500
H	-2.20209400	1.01970200	0.22584400
H	1.98445700	1.02945600	0.58963500
H	-0.32568500	1.58780600	-1.18983100
H	0.03334700	2.25220000	0.39447400

15
E(RB3LYP) = -558.277230 a.u.

N	-1.09554600	0.36908100	-0.00021300
O	-0.93879200	1.63673200	-0.00086500
C	-0.10901700	-0.49767600	0.00029900
H	-0.40589400	-1.53554800	0.00081400
C	-2.55431500	-0.15796900	0.00005900
C	-2.77192300	-0.98909300	1.27292500
H	-3.81936200	-1.29510300	1.32794800
H	-2.16065300	-1.89306300	1.28937600
H	-2.54228900	-0.39857700	2.16293500
C	-2.77111800	-0.99293400	-1.27047200
H	-3.81873200	-1.29826100	-1.32580400
H	-2.53990800	-0.40542000	-2.16204800
H	-2.16058900	-1.89745600	-1.28331500
C	-3.48702800	1.05347200	-0.00205900
H	-4.51690800	0.68969000	-0.00172700
H	-3.33390200	1.67406800	0.88018600
H	-3.33350800	1.67129700	-0.88618200
C	1.31341100	-0.21276800	0.00016500
C	2.18308700	-1.32513000	-0.00013200
C	1.88227400	1.07781900	0.00034800
C	3.56083500	-1.15836100	-0.00029500
H	1.76463000	-2.32603200	-0.00029200
C	3.26585800	1.23396300	0.00027300

H	1.22675300	1.93416800	0.00058300
C	4.11097800	0.12534400	-0.00007400
H	4.20782000	-2.02825600	-0.00059200
H	3.68655900	2.23348100	0.00047600
H	5.18688600	0.25760000	-0.00016600

TS1n

E(RB3LYP) = -791.681419 a.u.

1 imaginary frequency: -297.6929 cm^{-1}

N	0.54408400	-1.38586500	-0.29252900
O	0.45978000	-1.21292900	-1.56085300
C	-0.28904500	-0.73806500	0.53098900
C	0.50016700	1.26977600	0.23920800
C	0.52725100	1.63442400	-1.05347500
H	-0.08176500	-0.88145300	1.57995000
C	1.78278200	-2.13212500	0.18296900
C	1.83110500	-2.27046600	1.70720200
H	2.70593600	-2.87081600	1.96548400
H	1.93714200	-1.30689800	2.20999700
H	0.95108900	-2.78499300	2.10013100
C	3.01655600	-1.37154700	-0.32573500
H	3.91867800	-1.93127500	-0.06859100
H	2.97189500	-1.25543000	-1.40791700
H	3.07884200	-0.38174700	0.13135200
C	1.70079800	-3.52598000	-0.46259600
H	2.59985700	-4.09650600	-0.21965700
H	0.83195500	-4.07449400	-0.08976400
H	1.62040500	-3.43708900	-1.54545700
C	-1.70614500	-0.44653100	0.22639900
C	-2.53098400	-0.11976400	1.31859800
C	-2.28585800	-0.50956000	-1.05163700
C	-3.88637100	0.13153000	1.14441100
H	-2.10096700	-0.06671900	2.31328900
C	-3.64864000	-0.26666100	-1.21823300
H	-1.66008500	-0.75516000	-1.89584700
C	-4.45403600	0.05844000	-0.12876400
H	-4.50132900	0.38010300	2.00211100
H	-4.08039700	-0.32648900	-2.21132800
H	-5.51118900	0.25417700	-0.26786000
C	1.57570500	3.73668000	-0.36364100
C	1.45871400	3.31581300	1.13006000
C	1.05567400	1.85485500	1.29773600
C	1.70427300	2.53909200	-1.35751100
H	0.78057600	3.99697400	1.65634400
H	1.36017100	1.33145400	2.19910600
H	-0.32340100	1.58251200	-1.72134800
H	2.65791400	2.02619500	-1.19920400
H	1.69017900	2.90558900	-2.38698000
H	2.43028300	3.42205900	1.62807900

H	0.69022200	4.31080800	-0.65144700
H	2.43548600	4.40421400	-0.48178700

TS1x
E(RB3LYP) = -791.680158 a.u.
1 imaginary frequency: -311.8109 cm^{-1}

C	-1.72951500	3.67576800	-0.23529600
C	-0.83073100	3.07713900	-1.35876000
C	0.08950000	1.97823700	-0.84545200
C	-0.29912500	1.37349600	0.28806000
C	-1.07532700	1.84494900	1.26789200
C	-1.24071600	3.35144100	1.20849600
H	-1.45786800	2.73766000	-2.19112600
H	1.05240000	1.83723700	-1.31564000
H	-1.71839200	1.23009100	1.88893600
H	-0.29573900	3.86793100	1.40627000
H	-1.97058700	3.70897500	1.93930900
H	-0.17995700	3.85433500	-1.77627200
H	-2.74691900	3.28694900	-0.33436000
H	-1.79180600	4.76059900	-0.36777400
N	1.41605300	-0.68542400	-0.30867200
O	1.28282800	-0.69093800	-1.58562700
C	0.34066000	-0.64813600	0.49406500
H	0.58174400	-0.64317100	1.54449900
C	2.85004300	-0.60801100	0.20355600
C	3.51724400	-1.92198000	-0.23890500
H	4.57244200	-1.91204700	0.04300800
H	3.03934400	-2.77962600	0.24117000
H	3.44177500	-2.03857900	-1.32009700
C	2.91753600	-0.46646500	1.72669300
H	3.96913300	-0.40211400	2.01395600
H	2.42394000	0.44267200	2.07699700
H	2.49092100	-1.32927500	2.24282200
C	3.53083500	0.59332700	-0.46835300
H	4.59318000	0.59548300	-0.21539900
H	3.42794900	0.53098800	-1.55099100
H	3.09340200	1.53302800	-0.12397600
C	-0.94398700	-1.31054800	0.17281800
C	-1.71636400	-1.75328700	1.26117800
C	-1.42369700	-1.54316100	-1.12705300
C	-2.92369900	-2.41562100	1.06164300
H	-1.35975700	-1.58641600	2.27221800
C	-2.62757100	-2.21651200	-1.32006600
H	-0.84249000	-1.19629800	-1.96705100
C	-3.38400600	-2.65347800	-0.23297900
H	-3.50056500	-2.75013200	1.91650800
H	-2.98063100	-2.39444800	-2.33001000
H	-4.32299400	-3.17132400	-0.39248700

TS2n
E(RB3LYP) = -791.677247 a.u.
1 imaginary frequency: -254.6151 cm^{-1}

C	-2.84209100	-2.90005500	0.81382700
C	-1.54080300	-2.43894000	1.53154100
C	-0.64864100	-1.54623500	0.66521900
C	-1.25031800	-1.02293000	-0.42623300
C	-2.31867700	-1.43542900	-1.12060500
C	-2.72976600	-2.84518400	-0.73521500
H	-1.81281200	-1.96458000	2.48442100
H	0.42220700	-1.62388500	0.78535800
H	-2.99910100	-0.77277000	-1.64433300
H	-1.98781400	-3.58270400	-1.06861500
H	-3.68582800	-3.12045400	-1.19028000
H	-0.94221800	-3.31707900	1.80166300
H	-3.67153200	-2.24771200	1.10563600
H	-3.10504600	-3.91108400	1.14685000
N	-0.17703900	1.37014800	-0.23511900
O	-0.59197800	0.48132600	-1.12939100
C	0.92694600	1.16373700	0.44967300
H	1.08436900	1.84005300	1.27574400
C	-1.15908100	2.49251400	0.05431000
C	-0.54822900	3.53272300	0.99941200
H	-1.25419800	4.36033500	1.08899800
H	-0.38382200	3.13777500	2.00427900
H	0.39049900	3.93670000	0.61361900
C	-2.42424400	1.88795700	0.68191400
H	-3.13642600	2.69135500	0.88346100
H	-2.89154400	1.16786800	0.01234000
H	-2.19278900	1.38867700	1.62504000
C	-1.47470100	3.14643700	-1.30060400
H	-2.21151400	3.93903400	-1.15424500
H	-0.57493200	3.58785200	-1.73632400
H	-1.87976000	2.41552500	-1.99879600
C	2.03312400	0.28373500	0.12923900
C	3.10626500	0.27001700	1.04690400
C	2.14144000	-0.50055600	-1.03888700
C	4.23830000	-0.49720200	0.81293300
H	3.04219600	0.87204800	1.94692100
C	3.28828000	-1.25195300	-1.27220200
H	1.33208200	-0.50431700	-1.75265600
C	4.33614900	-1.26167900	-0.35184200
H	5.04813200	-0.49495000	1.53325900
H	3.36062500	-1.84136500	-2.17923600
H	5.22060800	-1.85970300	-0.53845600

TS2x
E(RB3LYP) = -791.679910 a.u.
1 imaginary frequency: -259.6446 cm^{-1}

N	-1.52974800	-0.43140400	0.24801400
O	-1.09803300	0.40647700	1.15935300
C	-0.66002700	-1.10587500	-0.48233700
H	-1.06948800	-1.59496800	-1.35305200
C	-3.01687300	-0.34123900	-0.04951700
C	-3.42774200	-1.30939000	-1.16241300
H	-4.51163700	-1.25037900	-1.27887200
H	-2.98167200	-1.04896300	-2.12470100
H	-3.17674100	-2.34441600	-0.91959500
C	-3.35205000	1.10332000	-0.44594100
H	-4.43462100	1.20300100	-0.54985700
H	-3.01000100	1.80306600	0.31609200
H	-2.89258600	1.36761200	-1.40024000
C	-3.72654900	-0.72033100	1.26178600
H	-4.80763300	-0.63813100	1.13013200
H	-3.48999800	-1.74859600	1.54637700
H	-3.41974000	-0.05480200	2.06845300
C	0.69700700	-1.48147600	-0.11635800
C	1.45434400	-2.16581300	-1.08936900
C	1.26819200	-1.28888100	1.15811200
C	2.73219300	-2.63212200	-0.80696100
H	1.02805700	-2.33264800	-2.07296900
C	2.54092300	-1.77661100	1.43761600
H	0.70382600	-0.76693400	1.91569600
C	3.28255000	-2.44349600	0.46180900
H	3.29581000	-3.15162000	-1.57373500
H	2.95921700	-1.63008400	2.42740300
H	4.27678200	-2.81194900	0.68687200
C	2.49677100	2.58270900	-0.54468500
C	1.62523000	1.77340000	-1.55430100
C	0.20032800	1.52381300	-1.05423500
C	0.04602100	1.67728400	0.27401000
C	0.73226500	2.36840900	1.17492800
C	1.66745600	3.36814800	0.51360600
H	2.14591500	0.83786200	-1.80108600
H	-0.61025600	1.55544000	-1.77199100
H	0.84115000	2.08345700	2.21623000
H	1.10886000	4.17248900	0.02205300
H	2.33659500	3.83451100	1.24225600
H	1.53968800	2.32820200	-2.49549700
H	3.15136100	1.89570200	-0.00007800
H	3.14937800	3.26906700	-1.09531600

16a

E(RB3LYP) = -791.774759 a.u.

N	-0.16666500	1.21158300	-0.36727000
O	-1.63199000	1.18151200	-0.52962000
C	0.14778700	0.04162100	0.51163800

C	-1.04941600	-0.87061400	0.28810400
H	0.18345400	0.32436500	1.56995400
C	0.16477300	2.57201600	0.15104500
C	1.68420900	2.62960200	0.37518400
H	1.96554100	3.65153800	0.64041700
H	2.00683900	1.97449700	1.18659900
H	2.22478100	2.34744600	-0.53073700
C	-0.57736200	2.92918400	1.45452900
H	-0.32290900	3.94912300	1.75376700
H	-1.65697200	2.87003300	1.31424700
H	-0.29900300	2.26833400	2.27931900
C	-0.21385600	3.57340400	-0.95414800
H	0.07283300	4.58537000	-0.65675700
H	0.30492000	3.32485400	-1.88336400
H	-1.28723200	3.55990200	-1.14476400
C	1.47036300	-0.61424800	0.14196100
C	2.31431900	-1.08551000	1.15184700
C	1.84250800	-0.81171400	-1.19252500
C	3.50275900	-1.74614200	0.83937900
H	2.04384000	-0.93000600	2.19141300
C	3.03024600	-1.46798900	-1.50653800
H	1.20388500	-0.43437700	-1.98152600
C	3.86464600	-1.93980800	-0.49200900
H	4.14620800	-2.10253000	1.63619100
H	3.30683000	-1.61064300	-2.54551900
H	4.78965000	-2.44889900	-0.73827100
C	-3.52786700	-2.05469800	-0.45580200
C	-2.72720900	-2.65535900	0.71596600
C	-1.40881000	-1.96091400	0.95786500
C	-1.91723800	-0.19891200	-0.74199000
C	-3.38785800	-0.52425500	-0.53510300
H	-2.56312600	-3.72553300	0.54532000
H	-0.77355800	-2.35858200	1.74589600
H	-1.60529300	-0.47597000	-1.76103300
H	-3.72333800	-0.06099800	0.39862000
H	-3.99563200	-0.11992400	-1.34869200
H	-3.31612200	-2.59583000	1.64141700
H	-3.17372500	-2.48898700	-1.39754900
H	-4.58125800	-2.33034200	-0.36352100

16b

E(RB3LYP) = -791.761112 a.u.

C	3.70349300	-0.74745600	0.69484000
C	3.07030300	0.62983400	0.99880600
C	1.95519300	1.02051700	0.01021100
C	1.43063500	-0.10492800	-0.84701700
C	2.21952000	-1.08343600	-1.27917400
C	3.65397900	-1.12199400	-0.80210800
H	2.65002000	0.63221400	2.00785300

H	2.30625200	1.82718800	-0.64880100
H	1.83911700	-1.89066500	-1.89807700
H	4.28279400	-0.43274600	-1.38179500
H	4.07562100	-2.11941700	-0.94936200
H	3.83983200	1.40522000	0.97673400
H	3.16697800	-1.52563200	1.24566600
H	4.73598100	-0.75883500	1.05398800
N	-0.18554800	1.47865200	-0.41592400
O	0.77772200	1.48982300	0.68406800
C	-0.07254900	0.09847000	-0.98457000
H	-0.36458600	0.17860400	-2.03431300
C	-1.45237100	2.11194400	0.01963700
C	-2.08687800	1.51482700	1.29200800
H	-2.93502400	2.13347500	1.59887400
H	-2.44939900	0.50040100	1.13116000
H	-1.36491400	1.49887600	2.11026500
C	-2.42901300	2.01495200	-1.16388200
H	-3.32158600	2.60484600	-0.94310500
H	-1.97421500	2.41139100	-2.07530200
H	-2.74677200	0.98754400	-1.34861200
C	-1.12210800	3.59649100	0.27217400
H	-2.03234700	4.14539300	0.52728900
H	-0.41336800	3.70249800	1.09462400
H	-0.68244700	4.04478400	-0.62199800
C	-0.86440100	-1.04968500	-0.36147200
C	-1.85896100	-1.68799400	-1.10850400
C	-0.60375300	-1.51578200	0.93513100
C	-2.58882400	-2.75236900	-0.57610300
H	-2.06408300	-1.35356200	-2.12059000
C	-1.33418400	-2.57087500	1.47230700
H	0.17080500	-1.04306200	1.52585600
C	-2.33171200	-3.19415200	0.71892900
H	-3.35362500	-3.23422600	-1.17514100
H	-1.12241300	-2.91338800	2.47934100
H	-2.89577000	-4.02023900	1.13708700

17a

E(RB3LYP) = -791.774353 a.u.

C	-2.61297000	-2.49266200	0.84022300
C	-1.20367100	-2.42550100	0.22806600
C	-0.90316100	-1.07960300	-0.46888900
C	-2.08851600	-0.18710900	-0.64005600
C	-3.36718300	-0.55019500	-0.53949500
C	-3.68975100	-1.96951100	-0.12746000
H	-0.45015400	-2.62786000	0.99451200
H	-0.49898300	-1.27929400	-1.46821700
H	-4.16189800	0.17421100	-0.68047500
H	-3.77078700	-2.64130600	-0.99358400
H	-4.66766200	-1.99107400	0.36234400

H	-1.10585400	-3.22406600	-0.51275500
H	-2.65120700	-1.88928900	1.75357700
H	-2.82730400	-3.52596900	1.12940300
N	-0.21622300	1.17719200	-0.49664700
O	-1.65367100	1.08333600	-0.89486800
C	0.08437300	-0.09824900	0.20840100
H	-0.15788300	-0.04573400	1.27737700
C	-0.10418600	2.45248600	0.28333200
C	1.35916900	2.59808300	0.73120700
H	1.49002400	3.58394100	1.18373500
H	1.64112500	1.85027800	1.47415900
H	2.04080900	2.51596900	-0.11767700
C	-1.03924800	2.51316800	1.50593700
H	-0.92742100	3.48093800	2.00121000
H	-2.08207800	2.40220400	1.20631000
H	-0.80391800	1.74189200	2.24329900
C	-0.44037500	3.59687100	-0.68883400
H	-0.29955400	4.56020600	-0.19222500
H	0.21532200	3.55792700	-1.56221500
H	-1.47401700	3.53307100	-1.02967000
C	1.53143300	-0.52184800	0.04707100
C	2.21138700	-1.09468700	1.12564100
C	2.18834900	-0.41758900	-1.18453700
C	3.51921800	-1.55902300	0.97987300
H	1.71808900	-1.17336400	2.08902500
C	3.49520700	-0.87523800	-1.33047400
H	1.67422600	0.03816800	-2.02201000
C	4.16557600	-1.44952800	-0.24908600
H	4.03163500	-1.99953400	1.82783300
H	3.99301200	-0.78319900	-2.28955100
H	5.18349700	-1.80434400	-0.36444900

17b

E(RB3LYP) = -791.772262 a.u.

N	-1.32039900	-0.44527500	0.40126000
O	-1.44728400	0.91465400	0.99243700
C	-0.25199600	-0.35140800	-0.63755300
H	-0.59576300	-0.83923500	-1.54933800
C	-2.68254100	-0.87270300	-0.04425900
C	-2.55386600	-2.34302000	-0.48110800
H	-3.54772500	-2.74315200	-0.69435900
H	-1.95095800	-2.46001700	-1.38420200
H	-2.10427700	-2.94195700	0.31409200
C	-3.27447900	-0.01908000	-1.18103900
H	-4.28187600	-0.36860200	-1.42148300
H	-3.34546100	1.02901900	-0.88301600
H	-2.67948400	-0.08551100	-2.09556700
C	-3.60186500	-0.80723200	1.18750100
H	-4.58365400	-1.21599100	0.93650600

H	-3.18124300	-1.39328300	2.00825900
H	-3.73292500	0.21992700	1.52781500
C	1.01909800	-1.04475400	-0.17972000
C	1.81705600	-1.71233800	-1.11527300
C	1.43169600	-1.02225700	1.15745200
C	3.00545500	-2.33279800	-0.73080800
H	1.50232300	-1.75508900	-2.15343500
C	2.61889200	-1.64093000	1.54431200
H	0.80989000	-0.53454600	1.89761700
C	3.41166800	-2.29621100	0.60176800
H	3.60753600	-2.84939100	-1.47003400
H	2.92300300	-1.61625200	2.58505000
H	4.33256000	-2.78112100	0.90555400
C	2.01915900	2.56677900	-0.45740000
C	1.19948500	1.76612100	-1.48243900
C	-0.10953300	1.17798400	-0.90515600
C	-0.49554100	1.72240600	0.43268300
C	0.01976200	2.79983200	1.02496300
C	1.14590200	3.54569200	0.34655500
H	1.81521000	0.97365200	-1.91397400
H	-0.92242100	1.43035400	-1.59358900
H	-0.32727200	3.10632100	2.00582100
H	0.77035900	4.34038800	-0.31343800
H	1.75540100	4.04758400	1.10389100
H	0.93073400	2.43157900	-2.30823600
H	2.50309700	1.88109700	0.24530000
H	2.81388800	3.10741100	-0.98041700